Lack of FIBRILLIN6 in *Arabidopsis thaliana* affects light acclimation and sulfate metabolism

Kwanuk Lee[1], Martin Lehmann[1], Melanie V. Paul[2], Liangsheng Wang[1], Manja Luckner[3], Gerhard Wanner[3], Peter Geigenberger[2] (iD), Dario Leister[1] (iD) and Tatjana Kleine[1] (iD)

[1]Plant Molecular Biology (Botany), Department Biology I, Ludwig-Maximilians-University München, 82152, Martinsried, Germany; [2]Plant Metabolism, Department Biology I, Ludwig-Maximilians-University München, 82152, Martinsried, Germany; [3]Ultrastrukturforschung, Department Biology I, Ludwig-Maximilians-University München, 81252, Planegg-Martinsried, Germany

Summary

• *Arabidopsis thaliana* contains 13 fibrillins (FBNs), which are all localized to chloroplasts. FBN1 and FBN2 are involved in photoprotection of photosystem II, and FBN4 and FBN5 are thought to be involved in plastoquinone transport and biosynthesis, respectively. The functions of the other FBNs remain largely unknown.

• To gain insight into the function of FBN6, we performed coexpression and Western analyses, conducted fluorescence and transmission electron microscopy, stained reactive oxygen species (ROS), measured photosynthetic parameters and glutathione levels, and applied transcriptomics and metabolomics.

• Using coexpression analyses, *FBN6* was identified as a photosynthesis-associated gene. FBN6 is localized to thylakoid and envelope membranes, and its knockout results in stunted plants. The delayed-growth phenotype cannot be attributed to altered basic photosynthesis parameters or a reduced CO_2 assimilation rate. Under moderate light stress, primary leaves of *fbn6* plants begin to bleach and contain enlarged plastoglobules. RNA sequencing and metabolomics analyses point to an alteration in sulfate reduction in *fbn6*. Indeed, glutathione content is higher in *fbn6*, which in turn confers cadmium tolerance of *fbn6* seedlings.

• We conclude that loss of FBN6 leads to perturbation of ROS homeostasis. FBN6 enables plants to cope with moderate light stress and affects cadmium tolerance.

Introduction

Fibrillins (FBNs) owe their name to filament-like structures, called fibrils, that are involved in carotenoid storage in the chromoplasts of bell pepper fruits, in which they were first identified (Deruere *et al.*, 1994). The fibrils of bell pepper are formed from chloroplast plastoglobules during the chloroplast-to-chromoplast transition (Rottet *et al.*, 2015). Meanwhile, FBNs are generally described as plastid lipid-associated proteins (PAPs) which form a protein family found in photosynthetic organisms ranging from cyanobacteria to higher plants (Kessler *et al.*, 1999; Singh & McNellis, 2011; Nacir & Brehelin, 2013). *Arabidopsis thaliana* codes for 13 FBNs (Singh & McNellis, 2011); and as a 14th FBN, Singh & McNellis (2011) suggested FBN11 (At5g53450), whereas Lundquist *et al.* (2012) propose another FBN-like protein (At1g18060). All FBNs have been localized to chloroplasts, some of them more particularly to plastoglobules (Vidi *et al.*, 2006; Ytterberg *et al.*, 2006; Lundquist *et al.*, 2012). Plastoglobules are thylakoid-associated lipoprotein particles containing glycerolipids and several dozen proteins, whose functions were for long mostly unknown (Brehelin *et al.*, 2007; Singh &

McNellis, 2011; Lundquist *et al.*, 2012). Evidence has accumulated that plastoglobules are strongly associated with plastid metabolism, developmental transitions, and environmental adaptation (van Wijk & Kessler, 2017). Plastoglobules can be released from the thylakoid membrane by sonication, and purification based on their low density has facilitated the analysis of the metabolites and proteins they contain (Vidi *et al.*, 2006; Ytterberg *et al.*, 2006; Zbierzak *et al.*, 2010; Lundquist *et al.*, 2012). Plastoglobule proteome analyses have provided a clearer picture of the sub-chloroplast localization of FBNs (Vidi *et al.*, 2006; Ytterberg *et al.*, 2006; Lundquist *et al.*, 2012). Thus, FBN3a (At3g26070), FBN3b (At3g26080), FBN6 (At5g19940), FBN-like (At1g18060), and probably FBN9 (At4g00030) were found to be thylakoid-localized, FBN5 (At5g09820) and a truncated version of FBN7a (At3g58010) are located in the chloroplast stroma, and FBN10 (At1g51110) in thylakoids and plastoglobules. The remaining seven FBNs are localized to the plastoglobule core proteome, which in total comprises 30 proteins (Lundquist *et al.*, 2012). Furthermore, FBN6 is the only isoform that was found to be enriched in purified envelope fractions (Ferro *et al.*, 2010; Bouchnak *et al.*, 2019).

Plastid types vary in their FBN composition, suggesting that the various FBNs might have specialized functions in different classes of plastids (Singh & McNellis, 2011). Moreover, the FBNs have diverse molecular properties. Their molecular masses range from 21 to 42 kDa, their pI values vary between 4 and 9, and they possess different hydrophobicity profiles. This diversity suggests that each FBN family member has specific biological function(s) (Singh & McNellis, 2011; Lundquist et al., 2012). The first role assigned to members of the FBN family was an involvement in fibril structure formation. Thus, its founder member FBN1, which was purified from bell pepper chromoplasts together with carotenoids and polar lipids, can reconstitute the complete fibril structure in vitro (Deruere et al., 1994). Another proposed FBN function is based on the observation that some of the FBNs contain lipocalin domains, suggesting that FBNs may also play a role in metabolite transport (Singh & McNellis, 2011). Indeed, there is strong evidence that FBN4 (At3g23400) is involved in the partitioning of plastoquinone-9 (2,3-dimethyl-6-solanesyl-1,4-benzoquinone; PQ-9) between the plastoglobules and the rest of the chloroplast (Singh et al., 2012). Reduced PQ-9 levels are also found in Arabidopsis fbn5 knockout mutants, and interaction experiments, together with the seedling-lethal phenotype of fbn5 mutants, suggest that Arabidopsis FBN5 plays a critical role in PQ-9 biosynthesis, is essential for plant development (Kim et al., 2015), and plays a role as a transmitter of singlet oxygen (O) in the chloroplast stroma (Otsubo et al., 2018).

In addition to their proposed roles in structure formation and transport, it has been suggested that FBNs are involved in resistance to biotic stress (Singh et al., 2012) and in protecting PSII against photooxidative stress (Yang et al., 2006; Youssef et al., 2010; Otsubo et al., 2018). Thus, in Arabidopsis, ABA triggers accumulation of FBN1a (At4g04020), and ABA treatment and FBN1a overexpression both protect photosystem II (PSII) against photoinhibition triggered by light stress (Yang et al., 2006). Because no visually discernible growth phenotype was observed in Arabidopsis plants with either down or upregulated FBN1a levels, it was postulated that closely related members of the FBN family might functionally substitute for each other (Youssef et al., 2010). Consequently, RNA interference (RNAi) was employed to simultaneously downregulate FBN1a, FBN1b (At4g22240), and FBN2 (At2g35490) (Youssef et al., 2010). Under a combined high light and cold treatment, these plants display higher PSII photoinhibition, retarded shoot growth, lower anthocyanin accumulation, and an abnormal expression pattern of jasmonate-inducible genes. All these deficiencies can be neutralized by jasmonate treatment of RNAi plants, suggesting that FBN1 and FBN2 proteins modulate jasmonate biosynthesis during exposure to certain abiotic stresses (Youssef et al., 2010).

In this study, FBN6 was identified as a photosynthesis-associated gene by mining coexpression databases. To gain further insight into FBN6 function, an fbn6-1 transfer DNA (T-DNA) insertion mutant and artificial microRNA lines were characterized. Under normal growth conditions, fbn6 plants display delayed growth, have slightly reduced Chl contents, shorter primary roots, and are late flowering under long-day conditions. An FBN6-enhanced green fluorescent protein (eGFP) protein localizes to thylakoid and envelope membrane fractions, and FBN6 is needed to acclimate plants to moderate light stress. RNA sequencing (RNA-Seq) and metabolomics analyses point to accumulation of glutathione (GSH) in fbn6, which in turn confers cadmium (Cd) tolerance of fbn6 seedlings.

Materials and Methods

Plant material and growth conditions

The mutant lines fbn6-1 (GK_159E10; Col-0 background), fbn6-2, and fbn6-3 (GT_5_46738 and GT_5_46794; Ler background) were identified in the SIGnAL database (Alonso et al., 2003). Insertions were confirmed with the primers listed in Supporting Information Table S1.

Arabadopsis thaliana plants were grown on potting soil (Stender, Schermbeck, Germany) under controlled glasshouse conditions (daylight supplemented with illumination from HQI Powerstar 400W/D, providing a total photon fluence of $c.$ 120 µmol m^{-2} s^{-1} on leaf surfaces; 16 h : 8 h, light : dark cycle). Where indicated, seedlings were grown on agar (Sigma-Aldrich) plates containing half-strength Murashige and Skoog (MS) medium, 1.5% (w/v) sucrose and 0.3% (w/v) gelrite (Roth, Karlsruhe, Germany) at 22°C under 100 µmol m^{-2} s^{-1} provided by white fluorescent lamps. To investigate the effect of Cd on seedling growth, seeds were sown on MS medium supplemented with 50 or 250 µM cadmium chloride (CdCl$_2$), based on Cd concentrations applied in Chen et al. (2015).

Nucleic acid extraction

For DNA isolation, leaf tissue was homogenized in extraction buffer containing 200 mM Tris hydrochloride (Tris-HCl), pH 7.5, 25 mM NaCl, 25 mM EDTA, and 0.5% (w/v) sodium dodecyl sulfate (SDS). After centrifugation, DNA was precipitated from the supernatant by adding isopropanol. After washing with 70% (v/v) ethanol, the DNA was dissolved in distilled water.

For RNA isolation, frozen tissue was ground in liquid nitrogen (N). Total RNA was extracted with the RNeasy Plant Mini Kit (Qiagen, Hilden, Germany) according to the manufacturer's instructions. RNA quality and concentration and the A_{260}/A_{280} ratio were assessed by agarose gel electrophoresis and spectrophotometry. Isolated RNA was stored at −80°C prior to use.

Complementary DNA synthesis and real-time PCR analysis

Complementary DNA (cDNA) synthesis and real-time PCR analysis was performed as described (Scharfenberg et al., 2015) with the primers listed in Table S1. Whenever possible, primers were designed to flank intron sites to make it possible to discriminate amplification of genomic DNA.

Generation of artificial microRNA-mediated knockdown lines

Knockdown *fbn6-amiR* mutants were generated using an artificial microRNA (amiRNA)-mediated knockdown technique (Schwab *et al.*, 2006). The Web MicroRNA Designer program (http://wmd3.weigelworld.org/) was applied to generate two amiRNA constructs targeting different regions of *FBN6*. The amiR constructs were generated by PCR from pRS300 template vector with each primer combination of A + IV, III + II, and I + B mentioned in Table S1. The three products were amplified via PCR with A + B primers. The final products were cloned into pDONR207 via BP reactions (Thermo Fisher Scientific, Waltham, MA, USA) and were subsequently cloned via LR reactions (Thermo Fisher Scientific) into *pALLIGATOR3* (Bernaudat *et al.*, 2011). Arabidopsis transformation was conducted by the floral dip method using *Agrobacteruim tumefaciens* GV3101 strain (Clough & Bent, 1998). The individual T_1 seeds were selected by GFP fluorescence, and independent T_2 or T_3 transgenic lines were used for phenotypic analysis. Knockdown levels of T_2 *fbn6-amiR* lines were confirmed by reverse transcription (RT)-PCR and real-time PCR with the gene-specific primers listed in Table S1.

Expression and intracellular localization of fluorescence fusions

For overexpression of FBN6 in Col-0, the *AT5G19940.1* coding region was amplified from cDNA by PCR (see Table S1 for primer information). The PCR product was cloned with GATEWAY technology into pB7FWG2 to generate a fusion with eGFP under the control of the *Cauliflower mosaic virus* 35S promoter. The construct was introduced into Col-0 plants by floral dip (Clough & Bent, 1998).

For co-transformation experiments, the *VTE1* coding region was amplified from cDNA with primers listed in Table S1. The *Nco*I-digested product was cloned in frame 5 to the *dsRED* gene in the vector pGJ1425 (Jach *et al.*, 2001). Intact *A. thaliana* protoplasts were prepared as described (Dovzhenko *et al.*, 2003). For transient gene expression assays, 5×10^5 protoplasts were transfected with 20 µg of plasmid DNA by polyethylene glycol-mediated DNA uptake (Koop *et al.*, 1996) and cultured for 16 h at 22°C in the dark.

Fluorescence visualization was done as described (Xu *et al.*, 2017).

Leaf pigment analyses

For Chl extraction, approximately 10 mg of leaf tissue from 4-wk-old plants was ground in liquid N in the presence of 80% (v/v) acetone. After removal of cell debris by centrifugation, absorption was measured with an Ultrospec 3100 pro spectrophotometer (Amersham Biosciences, Freiburg, Germany). Pigment concentrations were calculated following Lichtenthaler (1987).

Relative anthocyanin levels were determined as described previously (Neff & Chory, 1998).

Chl fluorescence analysis

In vivo Chl*a* fluorescence of whole plants was recorded using an ImagingPAM Chl fluorometer (Heinz Walz GmbH, Effeltrich, Germany). Plants adapted to dark (for 20–30 min) were exposed to a pulsed, blue measuring beam (1 Hz, intensity 4; F_0) and a saturating light flash (intensity 4) to obtain $F_v/F_m = (F_m - F_0)/F_m$ (maximum quantum yield of PSII). Plants were exposed to actinic light (111 µmol m^{-2} s^{-1}) to record the induction curve of the effective quantum yield of PSII (ϕ_{II}). To quantify nonphotochemical quenching (NPQ) of Chl fluorescence (NPQ; $(F_m - F_m')/F_m'$), *in vivo* Chl*a* fluorescence was measured using the ImagingPAM as well as the Dual-PAM 100 (Heinz Walz GmbH).

Protein isolation and immunoblot analyses

Proteins were homogenized in 2× SDS sample buffer (62.5 mM Tris-HCl, pH 6.8, 20% (v/v) glycerol, 4% (w/v) SDS, 100 mM DTT, 0.05% (w/v) bromophenol blue), incubated for 7 min at 75°C and centrifuged for 15 min. Proteins were fractionated in a 10% (w/v) SDS polyacrylamide gel and transferred to polyvinylidene fluoride membranes (Millipore). Filters were then incubated with antibodies specific for the respective photosystem I (PSI) and PSII proteins (all obtained from Agrisera, Vännäs, Sweden). Signals were detected by enhanced chemiluminescence (ECL kit; Amersham Bioscience, Freiburg, Germany) using an ECL reader system (Fusion FX7; PeqLab, Life Science, VWR, Ismaning, Germany) and quantified using IMAGEJ (http://rsbweb.nih.gov/ij).

Chloroplast fractionation

Intact chloroplasts were isolated from fresh leaf material from *c.* 200 4-wk-old *CaMV35S::FBN6-GFP* (Col-0) plants grown under short-day conditions (16 h : 8 h, dark : light) according to Kauss *et al.* (2012). Fractionation of intact chloroplasts into thylakoids, stroma, and envelope was performed as described (Bouchnak *et al.*, 2018), as was the fractionation into plastoglobules and thylakoid membranes (Espinoza-Corral *et al.*, 2019).

RNA sequencing and data analysis

Total RNA from plants was isolated using Trizol (Invitrogen) and purified using Direct-zol™ RNA MiniPrep Plus columns (Zymo Research, Irvine, CA, USA) according to the manufacturer's instructions. RNA integrity and quality were assessed by an Agilent 2100 Bioanalyzer (Agilent, Santa Clara, CA, USA). Ribosomal RNA depletion, generation of RNA-Seq libraries, and 150 bp paired-end sequencing on an Illumina HiSeq 2500 system (Illumina, San Diego, CA, USA) were conducted at Novogene Biotech (Beijing, China) with standard Illumina protocols. Three independent biological replicates were used per genotype.

RNA-Seq reads were analyzed on the Galaxy platform (Afgan *et al.*, 2016) as described in Xu *et al.* (2019). Sequencing data

have been deposited in National Center for Biotechnology Information's Gene Expression Omnibus (Edgar *et al.*, 2002) and are accessible through GEO Series accession no. GSE125515.

Gas exchange measurements

CO_2 exchange measurements were conducted on whole rosettes from 4-wk-old plants using the portable GFS-3000 system (Heinz Walz GmbH). Conditions within the cuvette were set to 22°C, 60% relative humidity, and ambient CO_2 concentrations. The impeller speed was set to 7 and the flow rate to 750 µmol s^{-1}. Monitoring of the light curve was started with darkened rosettes. When the CO_2 and water system parameters had stabilized, the light level was progressively increased. The CO_2 assimilation rate per unit weight was calculated with the software GFS-WIN v.3.50b (Heinz Walz GmbH).

Transmission electron microscopy

Pieces of primary leaves were fixed with 2.5% (v/v) glutaraldehyde in fixative buffer (75 mM sodium cacodylate, 2 mM magnesium chloride, pH 7.0) and ultrathin sections were prepared as described (Romani *et al.*, 2015).

Metabolite analysis

Fresh material (25 mg) was ground in 180 µl cold (−20°C) methanol containing 5 µl ribitol (0.2 mg ml^{-1} in water) and 5 µl ^{13}C-sorbitol (0.2 mg ml^{-1} in water) as internal standards for the relative quantification. Samples (at least five independent replicates) were processed as described (Roessner *et al.*, 2001; Lisec *et al.*, 2006; Erban *et al.*, 2007). Finally, 1 µl of each sample was injected into a GC–time-of-flight MS system (Pegasus HT; Leco, St Joseph, MO, USA). Sample derivatization and injection were performed by an autosampler system (Combi PAL; CTC Analytics AG, Zwingen, Switzerland). Helium was used as carrier gas at a constant flow rate of 1 ml min^{-1}. Gas chromatography was conducted on an Agilent GC (7890A; Agilent) using a 30 m VF-5ms column with 10 m EZ-Guard column. The injection temperature of the split/splitless injector was set to 250°C, as well as the transfer line and the ion source. The initial oven temperature (70°C) was continuously increased to a final temperature of 350°C by a ramp of 9°C min^{-1}. Solvent delay was set to 340 s. Metabolites were ionized and fractionated by an ion pulse of 70 eV, and mass spectra were recorded at a rate of 20 s^{-1} within a scan range of 35–800 *m/z*. Chromatograms and mass spectra were evaluated using CHROMATOF 4.5 and TAGFINDER 4.1 software (Luedemann *et al.*, 2008). Nonpolar compounds were extracted as described (Espinoza-Corral *et al.* 2019).

Reactive oxygen species staining of rosette leaves

Reactive O species (ROS) staining was done essentially as described before (Lundquist *et al.*, 2013).

Quantification of glutathione

Extraction and determination of total and oxidized GSH content was essentially done as described (Queval & Noctor, 2007). Standard curves of GSH and oxidized GSH disulfide (GSSG) were prepared, and 25 mg of plant material was used.
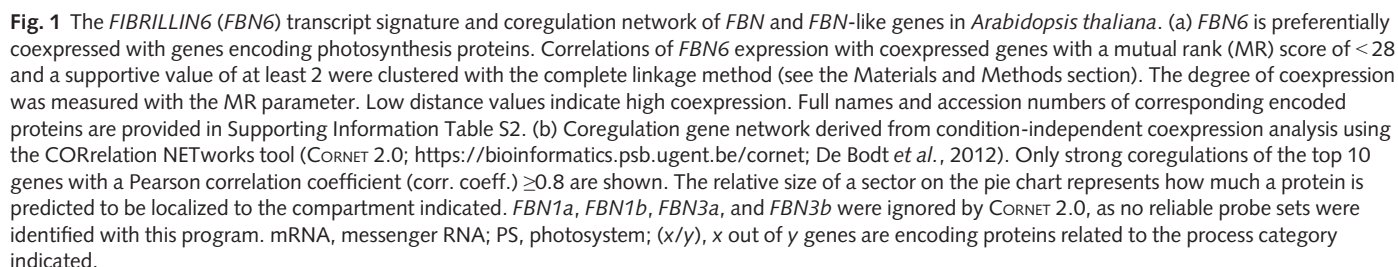
Data analysis

The significance of differences in gene expression in real-time PCR, root length, flowering time, and GSH content was evaluated by Duncan's multiple range test, Holm–Sidak test, or by Student's *t*-test, as indicated in the figure legends.

Results

FBN6 is co-regulated with photosynthesis genes

One means of identifying genes coding for proteins in particular pathways is the mining of coexpression data over a range of tissues and conditions (Usadel *et al.*, 2009). Here, we used photosynthesis genes as query genes in the ATTED-II CoExSearch tool (Aoki *et al.*, 2016) in an attempt to identify previously unrecognized photosynthesis-associated genes. We found that *FBN6* is coexpressed preferentially with genes coding for components of the photosynthetic machinery, like PSI reaction-center proteins, and components of the O-evolving and light-harvesting complexes (e.g. PsbY, PsbO1 and O2, Lhcb2.4, and Lhcb6) (Fig. 1a; Table S2). Furthermore, we used the CORrelation NETworks tool CORNET2.0 (De Bodt *et al.*, 2012), with which we constructed a condition-independent coexpression network (i.e. one based on the screening of all deposited microarray data, with no bias towards any particular type of condition/treatment) for 10 of the 14 *FBN*s (*FBN1a*, *FBN1b* and *FBN3a* and *FBN3a* were disregarded by CORNET2.0 because of their sequence similarity) and the FBN-like gene *At1G18060* (Lundquist *et al.*, 2012) (Fig. 1b). The *FBN11* gene is an outlier in this network and is only coexpressed with one gene of unknown function. The genes *FBN5* and *FBN8* are predominantly coexpressed with genes for chloroplast protein homeostasis and gene expression, respectively. Other *FBN* genes are coexpressed with genes for chloroplast proteins that are involved in several processes. The *FBN6* gene is the only *FBN* that is coexpressed chiefly with genes for photosynthesis proteins (Fig. 1b).

To assess to what extent *FBN* messenger RNA (mRNA) levels are regulated in response to various experimental perturbations, the GENEVESTIGATOR Perturbations Tool was applied. *FBN11* expression is most susceptible to perturbations: 285 conditions provoke at least a two-fold change in transcript level (Fig. 2). *FBN7a* and *FBN2* are least susceptible to perturbations, responding to only 30 and 38 conditions, respectively. *FBN6* is changed in 188 conditions, and most closely resembles *FBN5, 8, 10*, and *FBN-LIKE* (Fig. 2). *FBN6* is preferentially repressed upon treatment with flagellin 22 (a bacterial elicitor), lincomycin (an inhibitor of organellar translation), or norflurazon (an inhibitor of carotenoid synthesis) and under cold and high light

Fig. 1 The *FIBRILLIN6* (*FBN6*) transcript signature and coregulation network of *FBN* and *FBN*-like genes in *Arabidopsis thaliana*. (a) *FBN6* is preferentially coexpressed with genes encoding photosynthesis proteins. Correlations of *FBN6* expression with coexpressed genes with a mutual rank (MR) score of < 28 and a supportive value of at least 2 were clustered with the complete linkage method (see the Materials and Methods section). The degree of coexpression was measured with the MR parameter. Low distance values indicate high coexpression. Full names and accession numbers of corresponding encoded proteins are provided in Supporting Information Table S2. (b) Coregulation gene network derived from condition-independent coexpression analysis using the CORrelation NETworks tool (Cornet 2.0; https://bioinformatics.psb.ugent.be/cornet; De Bodt *et al.*, 2012). Only strong coregulations of the top 10 genes with a Pearson correlation coefficient (corr. coeff.) ≥0.8 are shown. The relative size of a sector on the pie chart represents how much a protein is predicted to be localized to the compartment indicated. *FBN1a*, *FBN1b*, *FBN3a*, and *FBN3b* were ignored by Cornet 2.0, as no reliable probe sets were identified with this program. mRNA, messenger RNA; PS, photosystem; (*x/y*), *x* out of *y* genes are encoding proteins related to the process category indicated.

conditions. This expression profile is shared with numerous photosynthesis-associated genes.

Identification and phenotypic analysis of the *fbn6-1* mutant and *fbn6* artificial microRNA lines

To learn more about the physiological functions of FBN6, loss-of-function *fbn6-1*, *fbn6-2*, and *fbn6-3* mutants were identified. In all mutants, the T-DNA insertion (*fbn6-1*) and the *Dissociation* (*Ds*) transposon (*fbn6-2*, GT_5_46738, and *fbn6-3*, GT_5_46794) were supposed to be located in the first exon of *FBN6*. However, we could only isolate homozygous *fbn6-1* mutants (Fig. 3a), and the *Ds* transposon insertions could not be confirmed. In *fbn6-1*, *FBN6* transcripts comprising sequences 5 of the insertion point were reduced to 1% of Col-0 levels and none were detectable 3 of the insertion (Fig. S1a). Growth of *fbn6-1* plants was retarded, as reflected in smaller rosettes and a reduction in rosette fresh weight to less than half that of Col-0 in 26-d-old plants (Fig. 3b). Moreover, *fbn6-1* plants were late flowering under long-day photoperiods (Fig. 3b), though not under short-day conditions (8 h : 16 h, light : dark cycles; Fig. S1b). Furthermore, leaves of *fbn6-1* appeared slightly paler than those of the wild-type (WT). Indeed, their Chl content was slightly but significantly reduced in *fbn6-1* plants, whereas the Chl*a*/Chl*b* ratio was increased (Fig. 3d). Segregation analysis of the F_2 offspring of *fbn6-1* back-crossed to Col-0 indicated that only one T-DNA inserted in *fbn6-1* was causing the *fbn6-1*-specific phenotype (Table S3). To ultimately confirm that the altered activity of *AT5G19940* was responsible for the mutant phenotype of *fbn6-1*, independent knockdown mutants of *FBN6* were generated by amiRNA (Schwab *et al.*, 2006) targeting the second (*amiR1*) and third exon of *AT5G19940* (*amiR2*) (Fig. S2a). Knockdown of *FBN6* was confirmed by RT-PCR (Fig. S2b) and real-time PCR analysis (Fig. S2c). Subsequent phenotypic analysis showed that *amiR1* and *amiR2* behaved like *fbn6* plants (Figs 3b,c, S2d,e). This indicates that the *fbn6* phenotype is indeed caused by knockout or knockdown of the *AT5G19940* gene.

Fig. 2 Clustering of transcriptional responses of *FIBRILLIN* (*FBN*) and *FBN*-like genes in *Arabidopsis thaliana*. The GENEVESTIGATOR Perturbations Tool was applied to all available *A. thaliana* microarrays. Number of samples, number of microarrays covering the different categories; number of perturbations, number of perturbations in which levels of the different *FBN* messenger RNAs are changed by at least two-fold.

Photosynthetic properties of *fbn6-1* mutant plants

To examine the effect of *FBN6* disruption on photosynthesis, Chl*a* fluorescence parameters were investigated. Under normal growth conditions, basic photosynthetic parameters, such as maximum (F_v/F_m) and effective (Φ_{II}) quantum yields of PSII, were slightly elevated in all developmental stages relative to Col-0 investigated (Fig. 4a,b), indicating that PSII and the electron transport chain are fully functional in *fbn6-1* and *amiR1* and *amiR2* plants. Also, a minor increase in NPQ was observed in *fbn6-1* mutants, both at the level of induction kinetics (111 µmol m^{-2} s^{-1}) and in response to increases in light intensity (Fig. S3a,b). This indicates that a slightly larger fraction of the absorbed light energy is dissipated as heat, but it does not explain the growth phenotype of plants lacking FBN6.

To determine the abundances of photosynthetic proteins in *fbn6-1*, immunoblot analysis was performed on total protein extracts from Col-0 and *fbn6-1* leaves. Representative subunits of PSI and PSII accumulated to similar levels in Col-0 and the *fbn6-1* mutant (Fig. 4c) – including PsaD and PsbO, whose genes are also coexpressed with *FBN6* (see Fig. 1a). Only levels of RbcL, the large subunit of Rubisco, were reduced in *fbn6-1* to approximately 75% of WT amounts (Fig. 4c). We therefore measured CO_2 assimilation rates in Col-0 and *fbn6-1* plants exposed to different light intensities up to 1000 µmol m^{-2} s^{-1}. However, no differences in CO_2 assimilation rates could be detected between Col-0 and *fbn6-1* rosettes (Fig. 4d).

Hence, loss of FBN6 has only a marginal effect on basic photosynthetic parameters, and CO_2 assimilation capacity is unaltered.

FBN6 is localized to thylakoid and envelope membranes

FBN6, together with FBN3a, FBN3b, FBN-like, and most probably FBN9, was found to be thylakoid localized (Lundquist *et al.*, 2012). Moreover, FBN6 is the only FBN isoform that was found to be enriched in purified envelope fractions (Ferro *et al.*, 2010), a localization that was recently supported by Bouchnak *et al.* (2019). To experimentally test for the subcellular location of FBN6, the fluorescence distribution in Col-0 protoplasts overexpressing the FBN6-eGFP fusion was investigated. The eGFP fluorescence signals colocalized with the Chl autofluorescence (Fig. 5a), confirming the localization of the FBN6 fusion protein to chloroplasts. However, the fluorescence signals were detected only occasionally as evenly distributed signals, and more often or exclusively as small dots suggestive of plastoglobules (Fig. 5a). To define the nature of the dots, and thereby confirm its localization to plastoglobules, FBN6-eGFP was cotransformed into *A. thaliana* protoplasts with a VTE1-dsRED construct. The localization of VTE1 (VITAMIN E DEFICIENT 1; a tocopherol cyclase) to plastoglobules was previously established in studies involving mass spectrometry and yellow fluorescent protein fusions (Vidi *et al.*, 2006; Lundquist *et al.*, 2012). Indeed, FBN6-eGFP signals were found in dots together with the dsRED signal of VTE1. Merging of both signals confirmed colocalization of FBN6 and VTE1, and thus suggested a localization of FBN6
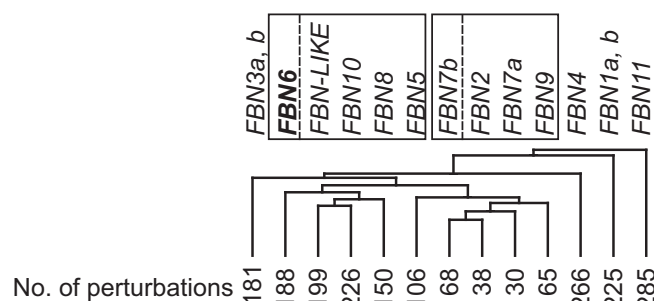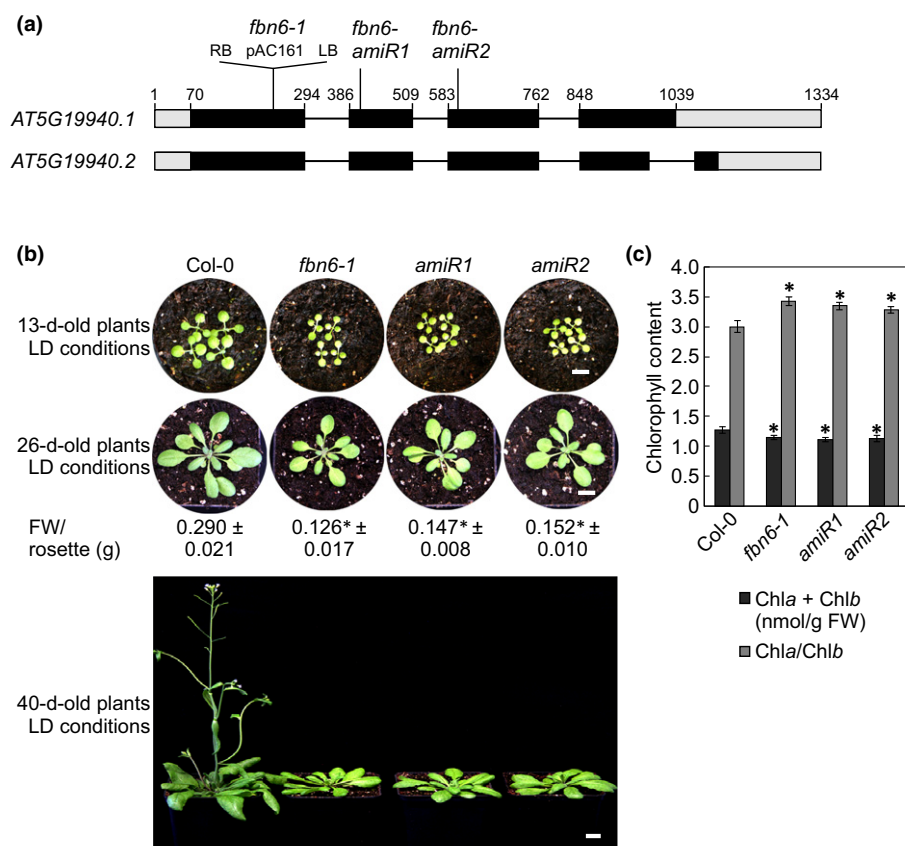
Fig. 3 Genetic and phenotypic characterization of the *Arabidopsis thaliana fibrillin6-1* (*fbn6-1*) and two artificial microRNA (*amiR1* and *amiR2*) mutant lines. (a) Schematic representation of transfer DNA (T-DNA) tagging of the *FBN6/AT5G19940* locus and target regions of the artificial microRNA constructs. Exons (black boxes), introns (black lines). and 5′ untranslated region (UTR) and 3′UTR (grey boxes) of the two different splice forms (*AT5G19940.1* and *AT5G19940.2*) according to The Arabidopsis Information Resource are shown. LB, left border; RB, right border. Nucleotides are numbered relative to the start of the 5′UTR. Locations and orientations of T-DNA and *Dissociation* insertion are indicated. The *fbn6-1* allele was identified in the GABI-Kat collection (Rosso *et al.*, 2003) as line GABI_152G06, which was donated to the SALK collection (Alonso *et al.*, 2003). (b) Phenotypes of 13, 26, and 40-d-old wild-type (Col-0) and *fbn6-1* plants grown in long-day (LD; 16 h : 8 h, light : dark cycle) conditions. Bar, 1 cm. (c) Determination of total Chl (Chl*a* + Chl*b*) concentration and the Chl*a*/Chl*b* ratio. Pigments were acetone-extracted, measured spectrophotometrically, and concentrations were determined as described (Lichtenthaler, 1987). The data are shown as mean values ± SD from four different plant pools. Significant differences between the data pairs were identified by the Student's *t*-test, and significant differences ($P < 0.05$) with respect to Col-0 are denoted by the asterisks.

to plastoglobules (Fig. 5a). However, FBN6 was found before to be localized to both thylakoids (Lundquist *et al.*, 2012) and envelope (Ferro *et al.*, 2010; Bouchnak *et al.*, 2019) fractions.

To further explore the issue of FBN6's localization, chloroplasts from Col-0 plants overexpressing FBN6-eGFP were prepared and thylakoid, stroma, and envelope-enriched fractions were isolated (Fig. 5b). These fractions were subjected to immunoblot analysis, and the enrichment of chloroplast subcompartments was tested by monitoring thylakoid light-harvesting Chl*a*/*b*-binding protein (LHCP), stromal RbcL, plastoglobular protein 18 (PG18; Espinoza-Corral *et al.*, 2019), and the translocon at the inner and outer envelope membrane proteins Tic110 and Toc64, respectively. RbcL was detected mainly in the stromal fraction, Tic110 and Toc64 mainly in the envelope fraction, PG18 nearly exclusively in the thylakoid fraction, and LHCP was most prominent in the thylakoids, but was also detected to a weaker extent in the envelope fraction (Fig. 5b), showing a contamination of the envelope fraction with thylakoids, but overall

corroborating the enrichment of the respective fractions. Using this approach, FBN6-eGFP was mainly detected in the thylakoid and, to a lesser extent, envelope membrane fractions. Comparing relative intensities of eGFP signals with those of LHCP, it was concluded that FBN6 was localized to thylakoids and the envelope, albeit to a weaker extent to the latter subcompartment. In a second fractionation approach, enrichment of selected fractions from a sucrose gradient used to fractionate into thylakoids and plastoglobules was tested by monitoring LHCP and PG18. LHCP was detected mainly in fractions 25–33 (Fig. 5c) and PG18 mainly in fraction 1. However, FBN6 was only detected in fractions co-migrating with LHCP, suggesting that FBN6 is not localized to plastoglobules, corroborating the previous finding of Lundquist *et al.* (2012).

Because FBN6-eGFP was localized to thylakoid and envelope membranes, we asked whether the growth phenotype of *fbn6-1* plants might be related to alterations in chloroplast ultrastructure. However, transmission electron microscopy (TEM) of
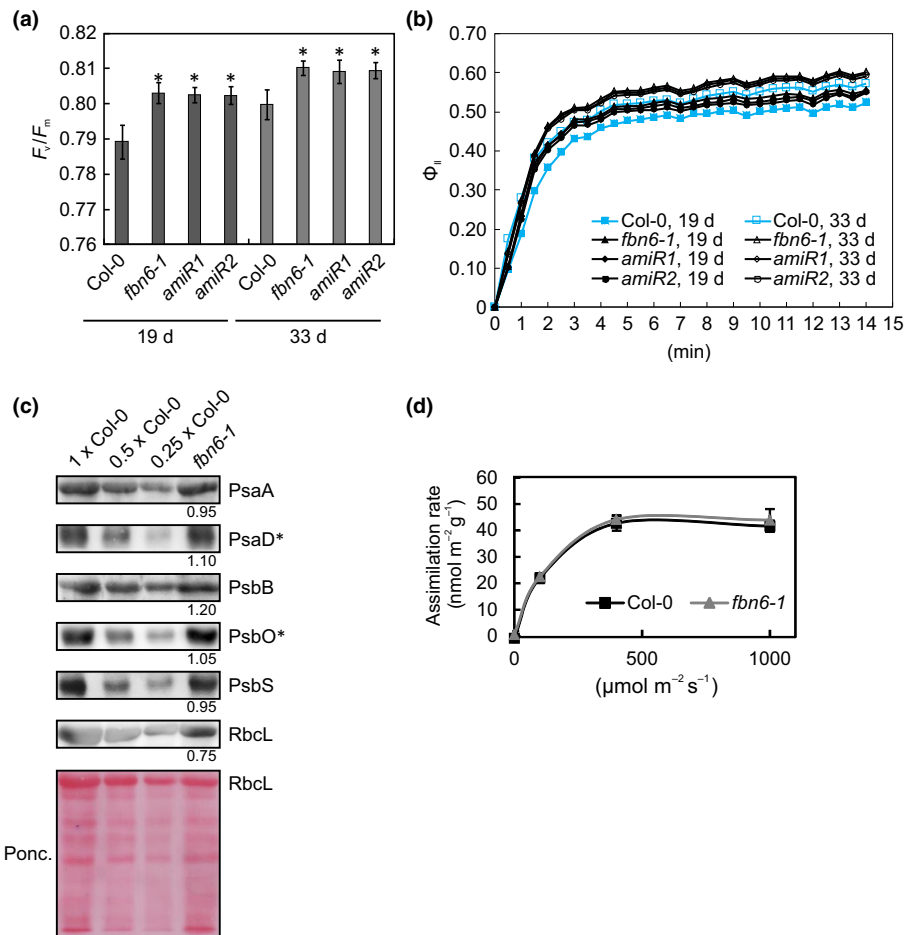
Fig. 4 Photosynthetic and gas exchange activity of *Arabidopsis thaliana* wild-type (Col-0) and *fibrillin6-1* (*fbn6-1*) and two artificial microRNA (*amiR1* and *amiR2*) mutant plants. (a) Maximum quantum yield of photosystem II (PSII) (F_v/F_m) of 19 and 33-d-old Col-0, *fbn6-1*, *amiR1*, and *amiR2* mutant plants. The data are shown as mean values $\pm$ SD of 8–10 different leaves. Significant differences between the data pairs were identified by the Student's *t*-test, and the asterisks denote significant differences ($P < 0.05$) with respect to Col-0. (b) Time course of induction of the effective quantum yield of PSII (Φ_{II}). Dark-adapted leaves (30 min) were illuminated for 14 min with 111 μmol m^{-2} s^{-1}. The data are shown as mean values $\pm$ SD from 8–10 different leaves. (c) Immunoblot analysis of selected chloroplast proteins. Total leaf protein extracts from wild-type (Col-0) and *fbn6-1* plants were fractionated by sodium dodecyl sulfate polyacrylamide gel electrophoresis, and blots were probed with antibodies raised against individual subunits of photosynthetic complexes. Decreasing levels of wild-type proteins were loaded in the lanes marked Col-0, 0.5× Col-0, and 0.25× Col-0. Loading was adjusted to FWs of leaf tissue. The Ponceau Red (Ponc.)-stained blot served as the loading control. Quantification of signals relative to Col-0 (=1.00) is provided below each *fbn6-1* panel. Asterisks mark proteins encoded by genes that are coexpressed with *FBN6*. (d) CO_2 assimilation rates of whole rosettes of wild-type (Col-0) and *fbn6-1* plants. CO_2 assimilation was measured at different light intensities in rosettes from plants grown under short-day conditions (8 h : 16 h, light : dark cycles) at 120 μmol m^{-2} s^{-1}. The data shown are mean values $\pm$ SD from four different plants.

ultrathin sections of primary leaves showed that the ultrastructures of chloroplasts and also that of plastoglobules were virtually indistinguishable between Col-0 and *fbn6-1* (Fig. S4).

In summary, FBN6-eGFP expression leads to localization of the fusion protein to thylakoid and envelope membranes, but chloroplast ultrastructure in *fbn6-1* mutants is indistinguishable from WT under normal growth conditions.
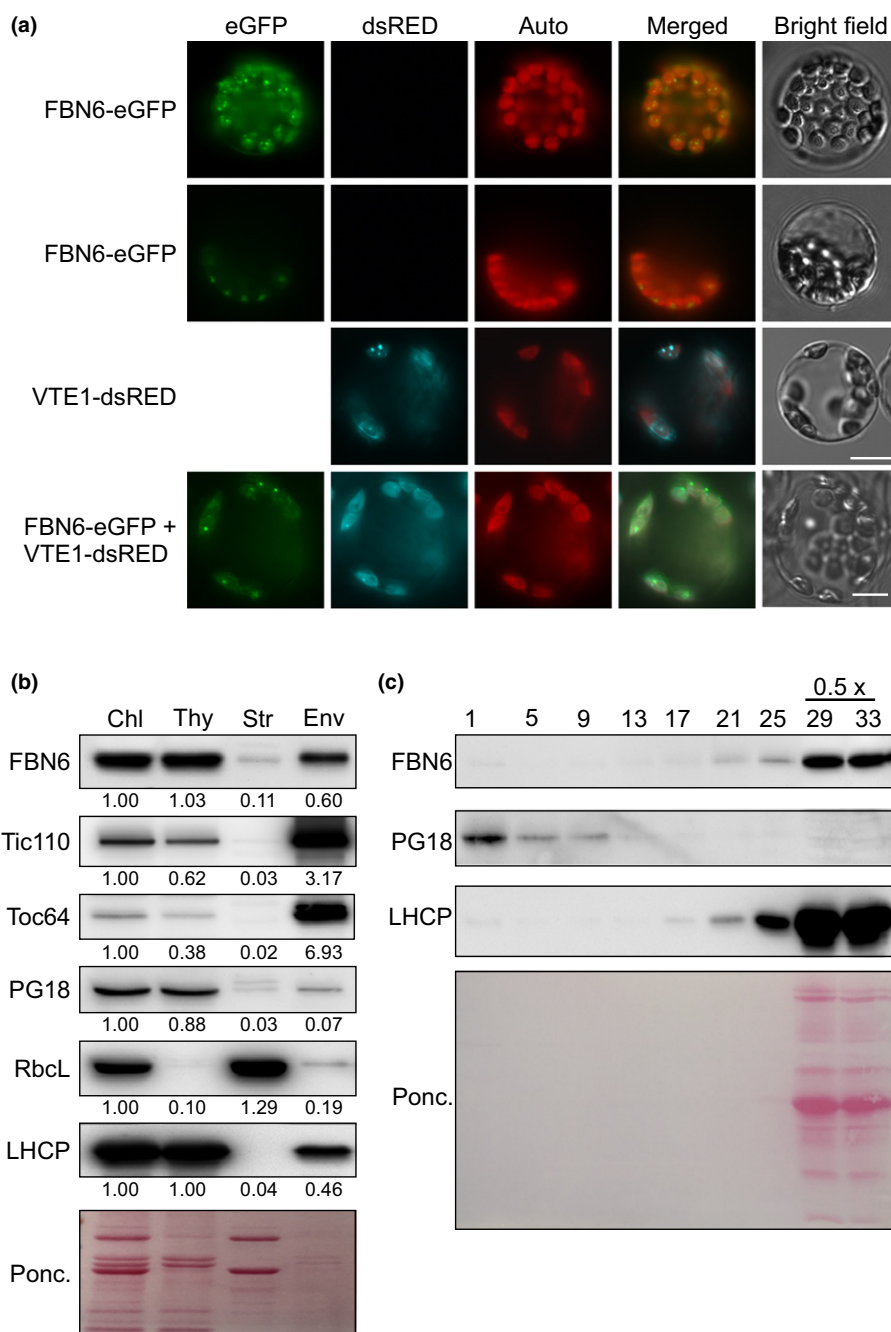
FBN6 is needed to acclimate plants to moderate light stress

GENEVESTIGATOR analysis indicated that *FBN6* mRNA levels are downregulated after 1200 μmol m^{-2} s^{-1} (HL) treatment. To confirm this, 29-d-old Col-0 plants grown under standard lighting conditions (120 μmol m^{-2} s^{-1}; GL) were exposed for 2 h to the 10-fold higher light level (HL) and real-time PCR analysis

showed that *FBN6* transcripts were indeed downregulated after HL treatment (Fig. S5a). Apparently, *FBN6* transcripts must be downregulated to accommodate the plant to the unfavorable HL condition, and we therefore asked whether a complete lack of FBN6 might help the plants to cope even better with HL stress. However, F_v/F_m values of *fbn6-1* plants exposed to 2 h of HL stress were only slightly lower than in Col-0 plants (Fig. S5b).

Moreover, ROS accumulation in plants grown in GL and transferred to 2 h of HL was visualized with nitroblue tetrazolium (NBT) and diaminobenzidine (DAB), stains specific for superoxide ($O_2^{\bullet-}$) and hydrogen peroxide (H_2O_2), respectively (Fig. S5c). Under GL conditions, rosette leaves of Col-0, *fbn6-1*, *amiR1*, and *amiR2* plants stained equally with NBT and DAB (Fig. S5c). After HL treatment, the NBT and DAB precipitates increased in Col-0 rosettes, whereas *fbn6-1* rosettes did not

Fig. 5 FIBRILLIN6 (FBN6) is localized to thylakoid and envelope membranes in *Arabidopsis thaliana*. (a) Fluorescence microscopy of *A. thaliana* protoplasts transiently expressing FBN6 fused to enhanced green fluorescent protein (eGFP; FBN6-eGFP). To visualize thylakoids and plastoglobules, protoplasts were (co)-transformed with VTE1-dsRED (dsRed, *Discosoma* red fluorescent protein). The eGFP fluorescence is shown in green (eGFP), dsRED fluorescence in cyan (dsRED), autofluorescence of chloroplasts in red (Auto). Bars, 10 µm. (b) Chloroplasts (Chl) were isolated from a 4-wk-old *CaMV35S::FBN6-eGFP* (Col-0) plants and fractionated into thylakoids (Thy), stroma (Str), and envelope (Env). These fractions were subjected to sodium dodecyl sulfate polyacrylamide gel electrophoresis, transferred to a polyvinylidene difluoride membrane, and exposed to antibodies raised against GFP (to detect the FBN6-eGFP fusion protein), Tic110 and Toc64 (as controls for the envelope fraction), PG18 (a plastoglobule-localized protein), RbcL (as a control for stromal proteins), or light-harvesting Chl*a/b*-binding protein (LHCP; as a control for the thylakoid fraction). Quantification of signals relative to the whole chloroplast fraction (=1.00) is provided below each panel and serves as an enrichment factor. The Ponceau Red (Ponc.)-stained blot served as the loading control. (c) Chloroplast membranes were isolated from 5-wk-old *CaMV35S::FBN6-eGFP* (Col-0) plants. The samples were fractionated on a discontinuous sucrose gradient, and fractions containing the same volume were taken from the top (number 1) to the bottom of the gradient. Selected fractions were treated as described in (b) with antibodies raised against GFP, PG18, and LHCP.

display darker stains (Fig. S5c). This might suggest that plants lacking FBN6 cannot properly adjust their ROS levels to HL conditions. However, under prolonged light stress, both genotypes responded in a similar manner (Fig. S5d).

Plants at 26 d old were also exposed to more moderate light stress (400 µmol m^{-2} s^{-1}; ML) combined with mild heat stress of 28°C for several days. After 6 d of ML, the leaf petioles of Col-0, *fbn6-1*, *amiR1*, and *amiR2* plants were shortened, leaf area expanded, and the maximum quantum yield of PSII was mildly reduced, but otherwise Col-0 plants still looked healthy (Fig. 6a). By contrast, the primary leaves of plants lacking FBN6 displayed small necrotic lesions and the reduction in F_v/F_m was more pronounced (Fig. 6a). Furthermore, older leaves of *fbn6* mutant lines

almost completely failed to induce anthocyanin accumulation: anthocyanin content was only 10% of WT levels (Fig. 6a).

To determine the impact of FBN6 deficiency on the ultra-structure of chloroplasts after 6 d of ML, TEM of ultrathin sections of Col-0 and *fbn6-1* primary leaves was conducted (Fig. 6b). Col-0 leaves showed well-developed lenticular chloroplasts with starch accumulating. Occasionally, grana thylakoids were somewhat distorted, indicating that Col-0 chloroplasts were under mild stress, but plastoglobules were present in normal numbers and size. The *fbn6-1* chloroplasts tended to be more nearly spherical in shape and contained no starch, and the diameter of grana stacks was smaller than in the WT. Obviously, the number of plastoglobules in *fbn6-1* chloroplasts increased, the

plastoglobules clustered, were larger, and variable in size. Along with the larger size, the core of the plastoglobules stained lighter, whereas the periphery was electron dense (Fig. 6b), indicating that *fbn6-1* chloroplasts in primary leaves already experience stress under moderate higher light conditions.

Identification of other mutants with an *fbn6-1*-like phenotype

To identify mutants with an *fbn6-1*-like phenotype, we filtered a comprehensive dataset of genes with a loss-of-function mutant phenotype in *A. thaliana* published in 2012 (Lloyd & Meinke, 2012) and identified 16 mutants (Table S4). The majority (12) of the mutants are impaired in genes for chloroplast-localized proteins. One of the mutants harbors a T-DNA insertion in *LHCB6*, which is coexpressed with *FBN6* (see Fig. 1b). Nearly half of the tagged genes encode proteins involved in ROS production/homeostasis, like the chloroplast ferredoxin AtFD2 and the chloroplast NADPH-dependent thioredoxin reductase NTRC, and the cytosolic ascorbate peroxidase APX1 which scavenges H_2O_2 (Dietz *et al.*, 2016). Indeed, genes encoding the following ROS-associated proteins are among the top 30 genes coexpressed with *FBN6*: thioredoxin F2, the GSH peroxidase GPX1, and the (cation exchanger) CAT1-interacting protein CXIP1 (AtGRXcp), which is a chloroplast glutaredoxin and is critical for protection against protein oxidative damage (Cheng *et al.*, 2006). Furthermore, mutants defective in tocopherol (vitamin E) biosynthesis, specifically *vte2* and *vte4* (Bergmuller *et al.*, 2003; Sattler *et al.*, 2004), have an *fbn6*-like phenotype. Here, it is interesting to note that *VTE5* is also coexpressed with *FBN6* (see Fig. 1).

Taken together, these data suggest that changes in ROS homeostasis might be responsible for impaired light acclimation and the delayed growth phenotype of *fbn6-1*.

Transcriptome changes point to an alteration of sulfate reduction in *fbn6* plants

To obtain molecular insights into a potential function of FBN6 in ROS homeostasis and to follow the general RNA expression pattern of nucleus- and organelle-encoded genes, RNAs isolated from 3-wk-old WT and *fbn6-1* plants were subjected to RNA-Seq. The mRNA levels of 194 and 118 genes were significantly (more than 1.5-fold) reduced or elevated, respectively (Table S5). Expression changes of several transcripts were confirmed by real-time PCR analysis of 3-wk-old Col-0, *fbn6-1* and *fbn6-amiR1* and *amiR2* plants (Fig. 7a). Plastid and mitochondria-encoded transcripts were not changed. Gene Ontology (GO) analysis with DAVID (da Huang *et al.*, 2009) identified among the nuclear-encoded upregulated genes in *fbn6-1* no enriched GO terms in the 'cellular component' and 'molecular function' categories. But enrichment of genes encoding proteins for the 'biological process' GOs 'removal of superoxide radicals', 'chaperone-mediated protein folding', and those associated with response to stresses like high light, chitin, heat, cold, and salt stress were identified (Fig. S6a). This corroborates the aforementioned assumption that ROS homeostasis is perturbed in *fbn6* plants. For the

downregulated genes in *fbn6-1*, DAVID detected as highest fold enriched GOs in the three categories 'cellular component', 'biological process', and 'molecular function' as being 'chloroplast thylakoid', 'sulfate reduction', and 'adenylyl-sulfate reductase activity', respectively (Fig. S6b). In particular, the 80 and 120-fold enrichment of 'sulfate reduction' and 'adenylyl-sulfate reductase activity' was remarkable. Eighteen transcripts that were in several transcriptomics studies upregulated by sulfate deficiency were identified (Kopriva *et al.*, 2015), and 11 of these were not up but downregulated in the *fbn6-1* mutant (Fig. 7b). This might indicate that the sulfate assimilation status in *fbn6* is not deficiency but an excessive supply. Fig. 7(c) shows the transcriptome changes in the sulfate assimilation pathway in more detail. Sulfate assimilation is partitioned between the cytosol and chloroplast (Takahashi *et al.*, 2011; Bohrer *et al.*, 2014); and in *fbn6-1*, in particular, the transcripts for the chloroplast-localized ATP sulfurylase, adenosine 5′-phosphosulfate kinase, adenosine 5′-phosphosulfate reductase (APR), and sulfite reductase were downregulated. Those enzymes act in the sulfate assimilation pathway (Fig. 7c).

Taken together, these transcriptome changes point to an alteration of sulfate reduction when FBN6 is lacking.

Lack of FBN6 leads to higher glutathione accumulation and confers cadmium tolerance
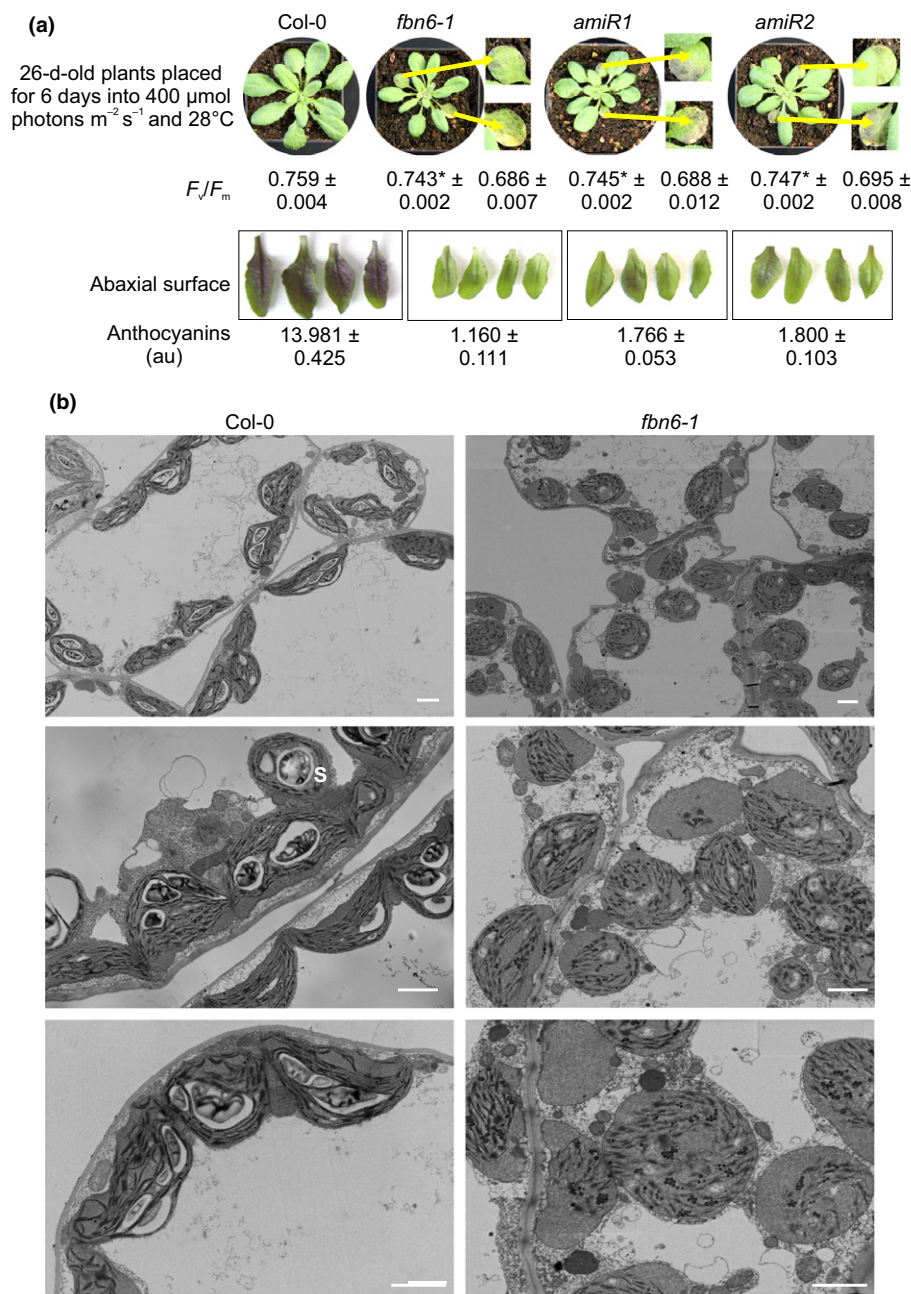
To examine the metabolic consequences of a lack of *fbn6*, GC–MS analysis was conducted on 3-wk-old Col-0 and *fbn6-1* mutant plants and 180 metabolites were identified (Table S6). Among the 36 metabolites that were significantly changed (> 1.5-fold change; $P < 0.05$) in *fbn6-1* compared with WT, glycine was 1.9-fold increased. Glycine is incorporated into γ-glutamylcysteine to yield GSH (Fig. 7c). Because suppressed *APR* mRNA expression has been found previously to be caused by increased GSH levels (Koprivova & Kopriva, 2014; Fu *et al.*, 2018), and indeed all three chloroplast-localized APRs were downregulated in *fbn6-1* (Fig. 7c; Table S5), we speculate that the increased glycine levels in *fbn6* might result in increased GSH levels. To test this, GSH content of 3-wk-old Col-0, *fbn6-1*, and *fbn6-amiR1* and *amiR2* plants was measured with a plate reader assay (Queval & Noctor, 2007). Indeed, all *fbn6* lines contained more total GSH (which is the sum of the reduced form of GSH and the oxidized GSSG) (Fig. 8a).

GSH is a key player in antioxidant mechanisms (Noctor *et al.*, 2018) and plays, for example, a pivotal role in Cd detoxification and tolerance (Liu *et al.*, 2016). We reasoned that the higher GSH content in *fbn6* might lead to enhanced Cd tolerance. To test this, Col-0, *fbn6-1*, and *fbn6-amiR1* and *amiR2* mutant seeds were germinated on control MS medium and on MS medium containing 50 or 250 μM $CdCl_2$, and phenotypes were scored after 14 d (Fig. 8b,c). When grown on MS plates, the primary root length of seedlings lacking FBN6 was reduced relative to Col-0 (Fig. 8c). By contrast, on MS supplemented with 50 μM $CdCl_2$, root lengths of *fbn6-1* and *fbn6-amiR* lines were approximately two-fold longer than for Col-0 (Fig. 8c), and growth of *fbn6* seedlings was significantly better than that of WT seedlings on plates supplemented with 250 μM $CdCl_2$. Thus, the mutants

Fig. 6 Behavior of *Arabidopsis thaliana* wild-type (Col-0) and *fibrillin6-1* (*fbn6-1*) and two artificial microRNA (*amiR1* and *amiR2*) mutant plants under moderate light stress. (a) Plants were first grown for 26 d under normal growth light (120 µmol m^{-2} s^{-1}) and then exposed to 400 µmol m^{-2} s^{-1} for the time periods indicated. Primary leaves of plants lacking FBN6 displayed small necrotic lesions (yellow arrow pointing to the enlargement of primary leaves displayed in square pictures) and maximum quantum yield of photosystem II (F_v/F_m) was more pronounced. The data are shown as mean values ± SD of 8–10 different leaves. Significant differences between the data pairs were identified by the Student's *t*-test, and the asterisks denote significant differences ($P < 0.05$) with respect to Col-0. The abaxial surface of leaves of plants grown under moderate light stress for 6 d reveals reduced anthocyanin accumulation in *fbn6-1* plants. Anthocyanins were extracted and measured photometrically; amounts are reported in arbitrary units (au). The asterisks indicate that values are statistically different between Col-0 and mutant plants based on Student's *t*-test ($P < 0.05$). (b) Representative transmission electron micrographs of ultrathin sections illustrate responses to moderate light stress in Col-0 and *fbn6-1* leaves. Primary leaves as accentuated for the *fbn6-1* mutant in (a) were harvested directly after onset of the light period. The Col-0 leaves show well-developed lenticular chloroplasts and plastoglobules of normal size. Plastoglobuli in *fbn6-1* chloroplasts stain with a biphasic contrast, are numerous, bigger, and variable in size. Moreover, the diameter of grana stacks is smaller, and chloroplasts have a globular shape. Starch grains are not accumulating in *fbn6-1* chloroplasts. G, grana; P, plastoglobule; S, starch grain. Bars, 4 µm.

were more resistant to Cd stress. Of note is that the increased GSH content of *fbn6* lines became even more prominent under 250 µM CdCl$_2$ stress than under control conditions (Fig. 8a,d).

In sum, these data show that a lack of FBN6 results in increased GSH levels and increased tolerance to Cd.

Discussion

Using coexpression information to identify new pathway components

Approaches to the identification of novel associated genes with pathways of interest include guilt-by-association approaches (Higashi & Saito, 2013). This approach is based on the assumption that genes which are coexpressed (i.e. show similar expression patterns over a range of different tissues and conditions) are likely to encode proteins that act in the same or closely related biological pathway(s) (Higashi & Saito, 2013; Yonekura-Sakakibara & Saito, 2013). For example, transcriptome and coexpression network analyses were exploited to identify HEAT INDUCIBLE LIPASE1 (HIL1) as a remodeler of chloroplastic monogalactosyldiacylglycerol under heat stress, and to show that *HIL1* homologue expression levels in various plants are tightly associated with chloroplastic heat stress responses (Higashi *et al.*, 2018).

With the ongoing expansion of public gene expression repositories, the predictive power and usefulness of coexpression information increases (Rung & Brazma, 2013), and many more studies have since made use of the abundance of microarray data
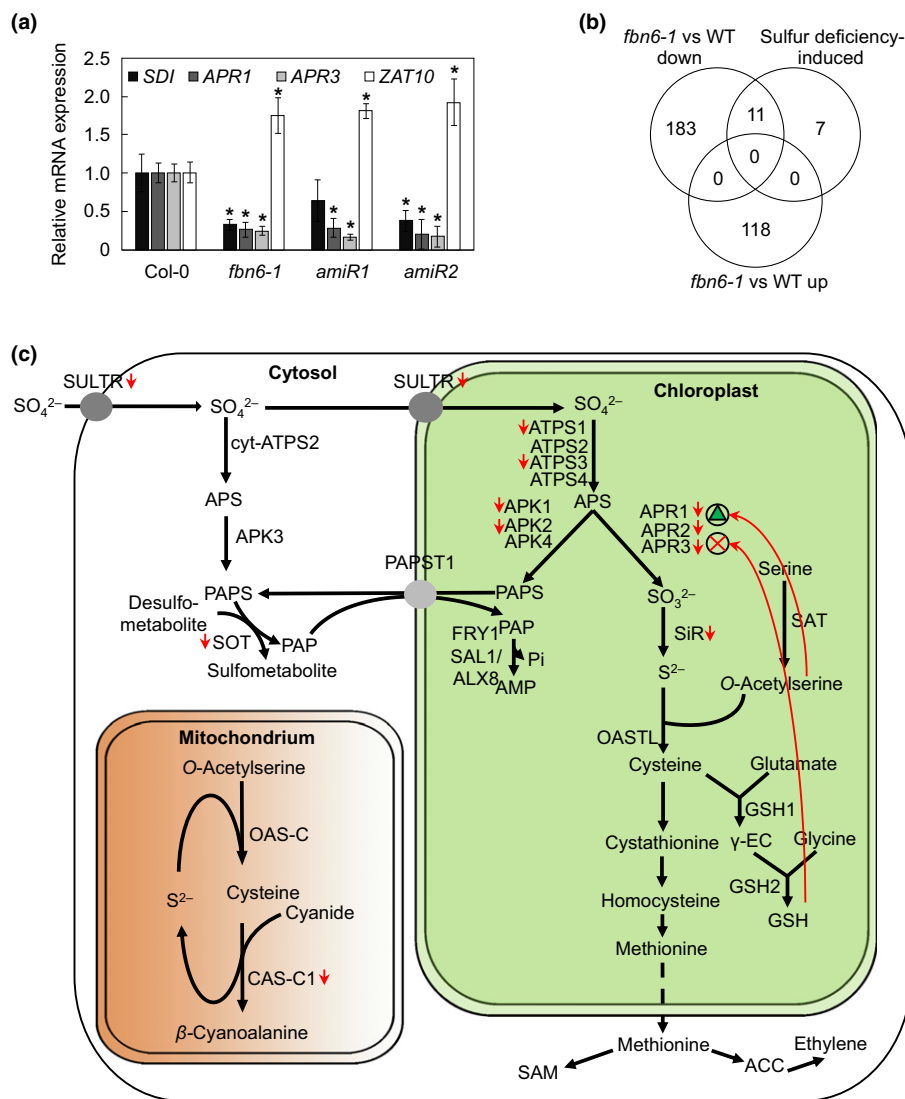
Fig. 7 Analysis of transcriptome changes in *Arabidopsis thaliana fibrillin6-1* (*fbn6-1*) mutant plants. (a) Real-time PCR analysis of 3-wk-old wild-type (Col-0), *fbn6-1*, and *fbn6-amiR1* and *amiR2* mutant plants. PCR was performed with primers specific for the genes of interest and *AT4G36800*, encoding an RUB1-conjugating enzyme (*RCE1*) as a control. The messenger RNA (mRNA) levels are expressed relative to that in the Col-0 control, which was set to 1. The results were normalized to the expression level of *AT4G36800*. Bars indicate SD. The asterisks indicate that values are statistically different between Col-0 and mutant plants based on the Student's *t*-test ($P < 0.05$). *APR*, *APS REDUCTASE*; *SDI*, *SULFUR DEFICIENCY INDUCED1*, a sulfate deficiency marker gene; *ZAT10*, *ZINC FINGER OF ARABIDOPSIS THALIANA10*, upregulated expression is associated with several stress responses, especially salt stress. (b) Venn diagram depicting the degree of overlap between the sets of genes whose expression levels were altered by at least two-fold (up or down) in the *fbn6-1* mutant compared with a robust set of sulfur-deficiency-induced genes extracted from Kopriva *et al.* (2015). (c) Sulfate assimilation leading to glutathione synthesis and sulfometabolites. Sulfate assimilation is partitioned between the cytosol and plastids (Takahashi *et al.*, 2011; Bohrer *et al.*, 2014). Sulfate is activated by reaction with ATP with the help of ATP sulfurylase (ATPS) to form adenosine 5′-phosphosulfate (APS), which is subsequently phosphorylated to 3′-phosphoadenosine 5′-phosphosulfate (PAPS) by APS kinase (APK) or reduced to sulfide by APS reductase (APR). The sulfide branch leads to glutathione synthesis in chloroplasts (Noctor *et al.*, 2012). Red arrows, direction of transcript changes encoding the respective enzymes; red cross, inhibition; green triangle, activation. γ-EC, γ-glutamylcysteine; GSH, glutathione; GSH1, γ-glutamylcysteine synthetase; GSH2, glutathione synthetase; OASTL, *O*-acetylserine(thiol)lyase; PAPST1, PAPS transporter; SiR, sulfite reductase; SULTR, sulfate transporter.

to identify new pathway components based on their coexpression with known elements. Here, we have used this methodology to identify *FBN6* as a putative photosynthesis and redox-associated gene. Subsequent definition of a coexpression network with all *FBN* genes and the *FBN-LIKE* gene showed that, of all *FBN*s, *FBN6* is the gene that is coexpressed with the largest number of photosynthesis genes (see Fig. 1a). Thus, it is coexpressed with various genes coding for the core photosynthetic apparatus and

regulators of photosynthesis, such as CURT1B (TMP14; see Table S2) or the O subunit of PSI that helps to balance excitation pressure between the two photosystems (Jensen *et al.*, 2004). The case of *psao* is an example of a mutant that fails to display a dramatic phenotype under normal-growth light conditions, although it is impaired in a photosynthesis-associated protein. Similarly, absence of Lhcb1 and Lhcb2 in antisense plants induces no significant growth phenotype, although Chl levels are
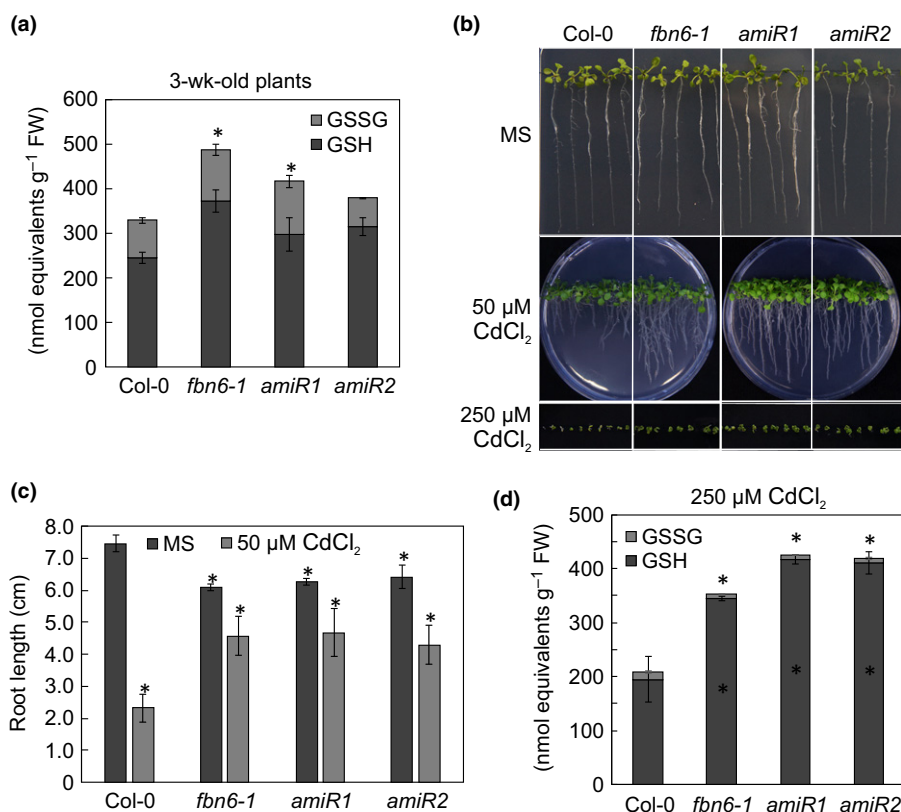
Fig. 8 Tolerance of *Arabidopsis thaliana* wild-type (Col-0), *fibrillin6-1* (*fbn6-1*), and *fbn6-amiR1* (*amiR1*) and *amiR2* mutant seedlings to cadmium stress (amiR, artificial microRNA). (a) Graph presenting the reduced glutathione (GSH) and glutathione dioxide (GSSG) content of 3-wk-old plants. Data are shown as mean values ± SD from six biological replicates. The significant difference (Holm–Sidak test; $P < 0.05$) is denoted by an asterisk. (b) Phenotypes of 14-d-old seedlings grown on control Murashige and Skoog (MS) plates and MS plates supplemented with 50 or 250 μM cadmium chloride (CdCl$_2$). (c) Graph presenting the root lengths of seedlings presented in (b). Data are shown as mean values ± SD from three independent experiments. Root lengths were measured and calculated with IMAGEJ (http://rsbweb.nih.gov/ij). The significant difference (Holm–Sidak test; $P < 0.05$) is denoted by an asterisk. (d) Graph presenting the reduced GSH and GSSG content of 14-d-old seedlings grown on MS plates supplemented with 250 μM CdCl$_2$. Data are shown as mean values ± SD from four biological replicates. The significant difference (Holm–Sidak test; $P < 0.05$) is denoted by an asterisk.

reduced (Andersson *et al.*, 2003). The *fbn6-1* mutant does show a phenotype under normal light conditions: it is stunted, contains slightly less Chl than Col-0, and is late flowering (see Figs 3, S1). But the *fbn6-1* growth phenotype cannot be accounted for either by altered basic photosynthesis parameters or by a reduced CO$_2$ assimilation rate (see Fig. 4).

FBN6 affects glutathione levels and cadmium tolerance

A large fraction of the mutants with an *fbn6-1*-like phenotype (see Table S3) are defective in ROS production/homeostasis. The chloroplast is considered to be the major source of ROS in plant cells. As a chloroplast-localized protein, FBN6 might be part of the ROS scavenging machinery. This would be compatible with our data, which point to an altered ROS homeostasis under HL conditions and altered transcript levels of genes for proteins involved in the removal of superoxide radicals in *fbn6-1* plants even under standard growth conditions (see Figs S5, S6). This suggests that an ROS-dependent signaling pathway is activated in the *fbn6-1* mutant under normally adequate growth conditions. Furthermore, anthocyanin levels in older *fbn6-1* leaves are reduced to 10% of WT levels under moderate light stress, whereas younger leaf tissue

of *fbn6-1* mutants appears to accumulate normal levels of anthocyanins. This phenotype is reminiscent of that of the *k1 k3* mutant, which is devoid of the plastoglobule kinases ABC1K1 and ABC1K3 (Lundquist *et al.*, 2013), and of the behavior of the *npq1* mutant (which lacks the xanthophyll cycle enzyme violaxanthin de-epoxidase; (Havaux *et al.*, 2000) and a mutant perturbed in two ascorbate peroxidases (Giacomelli *et al.*, 2007).

The perturbation in ROS homeostasis and the higher GSH content might explain the delayed growth phenotype of *fbn6* plants, as in the case of the *apx1* mutant, in which GSH is also increased (Jiang *et al.*, 2016). Indeed, the late-flowering (Pnueli *et al.*, 2003) and short-root phenotypes of *apx1* (Correa-Aragunde *et al.*, 2013) are also recapitulated by *fbn6-1* (see Figs 3, 8). Notably, flowering time is delayed by exogenous and endogenous GSH supply (Cheng *et al.*, 2015). GSH is used in several stress response pathways to detoxify ROS, xenobiotics, and certain heavy metals (Noctor & Foyer, 1998). Thus, it is most likely that the increased GSH content provokes Cd tolerance of *fbn6* plants (see Fig. 8). Accordingly, plants lacking APX1 are more tolerant to selenium (Jiang *et al.*, 2016), and the *sultr1;1 sultr1;2* mutant with lower GSH content is more sensitive to Cd (Liu *et al.*, 2016).

In general, oxidative stress – induced by treatment with paraquat, for instance – inhibits primary root elongation (Suzuki *et al.*, 2013). Among the other *fbn6*-like mutants identified in the filtered dataset referred to earlier (Lloyd & Meinke, 2012) are the mutants *vte2* (Sattler *et al.*, 2004) and *vte4* (Bergmuller *et al.*, 2003). Notably, root elongation is severely reduced in *vte2* plants and mildly compromised in the *vte1* mutant (Sattler *et al.*, 2004). Furthermore, *VTE5* is coexpressed with *FBN6* (see Fig. 1). Tocopherols are lipophilic antioxidants that are synthesized in all photosynthetic organisms; in plants, they are synthesized in plastids (Hussain *et al.*, 2013). To mitigate the harmful effects of elevated ROS, plants possess a complex network of enzymatic and nonenzymatic antioxidant defense systems, of which the latter involves low-molecular-weight antioxidants such as tocopherol, ascorbate, and GSH (Hussain *et al.*, 2013). When *vte1* or *vte2* leaf discs are simultaneously exposed to HL and low-temperature stress, they bleach and suffer from lipid photodestruction. Interestingly, this is not observed in whole plants exposed to long-term high light stress, unless the stress conditions are extreme (very low temperature and very HL), suggesting the availability of compensatory mechanisms for vitamin E deficiency under more physiological conditions (Havaux *et al.*, 2005). The *fbn6-1* mutant phenotype behaves very similarly to the WT under HL stress (see Fig. S5). It is conceivable that disruption of another part of the ROS network in combination with a lack of FBN6 might lead to a stronger phenotype, as has already been observed in other stress studies (Kanwischer *et al.*, 2005; Giacomelli *et al.*, 2007). For example, in *vte1*, ascorbate and GSH levels are increased. Whereas growth, Chl content, and photosynthetic quantum yield were very similar to WT in *vte1*, *vtc1* (ascorbate deficient), *cad2* (GSH deficient) and *vte1vtc1* mutants, they were clearly reduced in *vte1cad2* mutants, indicating that the simultaneous loss of tocopherol and GSH results in moderate oxidative stress, which in turn affects the stability and efficiency of the photosynthetic apparatus (Kanwischer *et al.*, 2005).

FBN6 is important for acclimation to light stress

Interestingly, VTE1 has been localized to plastoglobules; and, moreover, comparative analysis of chloroplast membrane fractions shows that plastoglobules are a site of vitamin E accumulation in chloroplasts (Vidi *et al.*, 2006). Meanwhile, it is clear that plastoglobules are not merely lipid stores, but are metabolically active, taking part in prenyl lipid metabolism, plastid biogenesis, environmental adaptation, and probably in other pathways (Vidi *et al.*, 2006; Ytterberg *et al.*, 2006; Brehelin *et al.*, 2007; Lundquist *et al.*, 2012; Nacir & Brehelin, 2013; Rottet *et al.*, 2015; van Wijk & Kessler, 2017). Under abiotic stress conditions like HL, heat, or cold, plastoglobules increase in size and number (Szymanska & Kruk, 2010; Zhang *et al.*, 2010; Heyneke *et al.*, 2013; Lundquist *et al.*, 2013).

Under a fluence of $400\,\mu mol\,m^{-2}\,s^{-1}$, although it has to be noted that FBN6 is not localized to plastoglobules (see Fig. 5), the plastoglobules in the *fbn6-1* mutant become larger than in the WT, which is a further indication that FBN6 is needed to acclimate Arabidopsis to moderate light stress. Apple trees or Arabidopsis with reduced mounts of FBN4 are also susceptible

to abiotic and biotic stresses (Singh *et al.*, 2010). In leaves of apple *fbn4* knockdown plants, the partitioning of PQ-9 between plastoglobules and the rest of the chloroplast seems to be disrupted; therefore, a failure to accumulate this antioxidant in plastoglobules might contribute to the increased stress sensitivity of *fbn4* knockdown trees (Singh *et al.*, 2012). Furthermore, plants in which mRNAs for FBN1a, FBN1b, and FBN2 were simultaneously downregulated by RNAi display higher PSII photoinhibition, retarded shoot growth, and lower anthocyanin accumulation under a combined HL and cold treatment (Youssef *et al.*, 2010), and it was recently shown that FBN5 is involved in the acclimation to photooxidative stress (Otsubo *et al.*, 2018).

Another example for the involvement of FBNs in plant growth regulation even under relatively nonstressful conditions is the FBN1 homologue C40.4 in potato. Under standard growth conditions, potato plants with reduced expression of C40.4 have reduced tuber size and yield, and their growth is stunted (Monte *et al.*, 1999). On the other hand, overexpression of bell pepper FBN1 in tobacco results in a greater plant height and accelerated flowering under higher light intensities ($300\,\mu mol\,m^{-2}\,s^{-1}$), but not under lower light intensities ($100\,\mu mol\,m^{-2}\,s^{-1}$) conditions (Rey *et al.*, 2000).

Thus, overall, a picture is emerging in which FBNs have important roles in plant responses to stresses.

Author contributions

Conceptualization, formal analysis, and supervision: TK; investigation: KL, M Lehmann, LW, MVP, M Luckner, GW and TK; writing of original draft: TK; writing review and editing: DL, PG and TK; funding acquisition: DL, PG and TK.

ORCID

Peter Geigenberger https://orcid.org/0000-0001-9512-349X
Dario Leister https://orcid.org/0000-0003-1897-8421
Tatjana Kleine https://orcid.org/0000-0001-6455-3470

References

Afgan E, Baker D, van den Beek M, Blankenberg D, Bouvier D, Cech M, Chilton J, Clements D, Coraor N, Eberhard C *et al.* 2016. The Galaxy platform for accessible, reproducible and collaborative biomedical analyses: 2016 update. *Nucleic Acids Research* 44: W3–W10.

Alonso JM, Stepanova AN, Leisse TJ, Kim CJ, Chen H, Shinn P, Stevenson DK, Zimmerman J, Barajas P, Cheuk R *et al.* 2003. Genome-wide insertional mutagenesis of *Arabidopsis thaliana*. *Science* 301: 653–657.

Andersson J, Wentworth M, Walters RG, Howard CA, Ruban AV, Horton P, Jansson S. 2003. Absence of the Lhcb1 and Lhcb2 proteins of the light-harvesting complex of photosystem II – effects on photosynthesis, grana stacking and fitness. *The Plant Journal* 35: 350–361.

Aoki Y, Okamura Y, Tadaka S, Kinoshita K, Obayashi T. 2016. ATTED-II in 2016: a plant coexpression database towards lineage-specific coexpression. *Plant and Cell Physiology* 57: e5.

Bergmüller E, Porfirova S, Dörmann P. 2003. Characterization of an *Arabidopsis* mutant deficient in γ-tocopherol methyltransferase. *Plant Molecular Biology* 52: 1181–1190.

Bernaudat F, Frelet-Barrand A, Pochon N, Dementin S, Hivin P, Boutigny S, Rioux JB, Salvi D, Seigneurin-Berny D, Richaud P *et al.* 2011. Heterologous expression of membrane proteins: choosing the appropriate host. *PLoS ONE* 6: e29191.

Bohrer AS, Kopriva S, Takahashi H. 2014. Plastid–cytosol partitioning and integration of metabolic pathways for APS/PAPS biosynthesis in *Arabidopsis thaliana*. *Frontiers in Plant Science* 5: e751.

Bouchnak I, Brugiere S, Moyet L, Le Gall S, Salvi D, Kuntz M, Tardif M, Rolland N. 2019. Unravelling hidden components of the chloroplast envelope proteome: opportunities and limits of better MS sensitivity. *Molecular & Cell Proteomics* 18, 1285–1306.

Bouchnak I, Moyet L, Salvi D, Kuntz M, Rolland N. 2018. Preparation of chloroplast sub-compartments from Arabidopsis for the analysis of protein localization by immunoblotting or proteomics. *Journal of Visualized Experiments* 140: 58581. https://doi.org/10.3791/58581.

Brehelin C, Kessler F, van Wijk KJ. 2007. Plastoglobules: versatile lipoprotein particles in plastids. *Trends in Plant Science* 12: 260–266.

Chen J, Yang L, Gu J, Bai X, Ren Y, Fan T, Han Y, Jiang L, Xiao F, Liu Y, Cao S. 2015. *MAN3* gene regulates cadmium tolerance through the glutathione-dependent pathway in *Arabidopsis thaliana*. *New Phytologist* 205: 570–582.

Cheng MC, Ko K, Chang WL, Kuo WC, Chen GH, Lin TP. 2015. Increased glutathione contributes to stress tolerance and global translational changes in Arabidopsis. *The Plant Journal* 83: 926–939.

Cheng NH, Liu JZ, Brock A, Nelson RS, Hirschi KD. 2006. AtGRXcp, an Arabidopsis chloroplastic glutaredoxin, is critical for protection against protein oxidative damage. *Journal of Biological Chemistry* 281: 26280–26288.

Clough SJ, Bent AF. 1998. Floral dip: a simplified method for *Agrobacterium*-mediated transformation of *Arabidopsis thaliana*. *The Plant Journal* 16: 735–743.

Correa-Aragunde N, Foresi N, Delledonne M, Lamattina L. 2013. Auxin induces redox regulation of ascorbate peroxidase 1 activity by *S*-nitrosylation/denitrosylation balance resulting in changes of root growth pattern in *Arabidopsis*. *Journal of Experimental Botany* 64: 3339–3349.

De Bodt S, Hollunder J, Nelissen H, Meulemeester N, Inzé D. 2012. CORNET 2.0: integrating plant coexpression, protein–protein interactions, regulatory interactions, gene associations and functional annotations. *New Phytologist* 195: 707–720.

Deruere J, Romer S, d'Harlingue A, Backhaus RA, Kuntz M, Camara B. 1994. Fibril assembly and carotenoid overaccumulation in chromoplasts: a model for supramolecular lipoprotein structures. *Plant Cell* 6: 119–133.

Dietz KJ, Turkan I, Krieger-Liszkay A. 2016. Redox and reactive oxygen species-dependent signalling in and from the photosynthesizing chloroplast. *Plant Physiology* 171: 1541–1550.

Dovzhenko A, Dal Bosco C, Meurer J, Koop HU. 2003. Efficient regeneration from cotyledon protoplasts in *Arabidopsis thaliana*. *Protoplasma* 222: 107–111.

Edgar R, Domrachev M, Lash AE. 2002. Gene Expression Omnibus: NCBI gene expression and hybridization array data repository. *Nucleic Acids Research* 30: 207–210.

Erban A, Schauer N, Fernie AR, Kopka J. 2007. Nonsupervised construction and application of mass spectral and retention time index libraries from time-of-flight gas chromatography–mass spectrometry metabolite profiles. *Methods in Molecular Biology* 358: 19–38.

Espinoza-Corral R, Heinz S, Klingl A, Jahns P, Lehmann M, Meurer J, Nickelsen J, Soll J, Schwenkert S. 2019. Plastoglobular protein 18 is involved in chloroplast function and thylakoid formation. *Journal of Experimental Botany* 70: 3981–3993.

Ferro M, Brugiere S, Salvi D, Seigneurin-Berny D, Court M, Moyet L, Ramus C, Miras S, Mellal M, Le Gall S *et al.* 2010. AT_CHLORO, a comprehensive chloroplast proteome database with subplastidial localization and curated information on envelope proteins. *Molecular & Cellular Proteomics* 9: 1063–1084.

Fu Y, Tang J, Yao GF, Huang ZQ, Li YH, Han Z, Chen XY, Hu LY, Hu KD, Zhang H. 2018. Central role of adenosine 5-phosphosulfate reductase in the control of plant hydrogen sulfide metabolism. *Frontiers in Plant Science* 9: e1404.

Giacomelli L, Masi A, Ripoll DR, Lee MJ, van Wijk KJ. 2007. *Arabidopsis thaliana* deficient in two chloroplast ascorbate peroxidases shows accelerated light-induced necrosis when levels of cellular ascorbate are low. *Plant Molecular Biology* 65: 627–644.

Havaux M, Bonfils JP, Lutz C, Niyogi KK. 2000. Photodamage of the photosynthetic apparatus and its dependence on the leaf developmental stage in the *npq1* Arabidopsis mutant deficient in the xanthophyll cycle enzyme violaxanthin de-epoxidase. *Plant Physiology* 124: 273–284.

Havaux M, Eymery F, Porfirova S, Rey P, Dormann P. 2005. Vitamin E protects against photoinhibition and photooxidative stress in *Arabidopsis thaliana*. *Plant Cell* 17: 3451–3469.

Heyneke E, Luschin-Ebengreuth N, Krajcer I, Wolkinger V, Muller M, Zechmann B. 2013. Dynamic compartment specific changes in glutathione and ascorbate levels in Arabidopsis plants exposed to different light intensities. *BMC Plant Biology* 13: e104.

Higashi Y, Okazaki Y, Takano K, Myouga F, Shinozaki K, Knoch E, Fukushima A, Saito K. 2018. *HEAT INDUCIBLE LIPASE1* remodels chloroplastic monogalactosyldiacylglycerol by liberating α-linolenic acid in Arabidopsis leaves under heat stress. *Plant Cell* 30: 1887–1905.

Higashi Y, Saito K. 2013. Network analysis for gene discovery in plant-specialized metabolism. *Plant, Cell & Environment* 36: 1597–1606.

da Huang W, Sherman BT, Lempicki RA. 2009. Bioinformatics enrichment tools: paths toward the comprehensive functional analysis of large gene lists. *Nucleic Acids Research* 37: 1–13.

Hussain N, Irshad F, Jabeen Z, Shamsi IH, Li Z, Jiang L. 2013. Biosynthesis, structural, and functional attributes of tocopherols *in planta*; past, present, and future perspectives. *Journal of Agricultural and Food Chemistry* 61: 6137–6149.

Jach G, Binot E, Frings S, Luxa K, Schell J. 2001. Use of red fluorescent protein from *Discosoma* sp. (dsRED) as a reporter for plant gene expression. *The Plant Journal* 28: 483–491.

Jensen PE, Haldrup A, Zhang S, Scheller HV. 2004. The PSI-O subunit of plant photosystem I is involved in balancing the excitation pressure between the two photosystems. *Journal of Biological Chemistry* 279: 24212–24217.

Jiang L, Chen Z, Gao Q, Ci L, Cao S, Han Y, Wang W. 2016. Loss-of-function mutations in the *APX1* gene result in enhanced selenium tolerance in *Arabidopsis thaliana*. *Plant, Cell & Environment* 39: 2133–2144.

Kanwischer M, Porfirova S, Bergmüller E, Dörmann P. 2005. Alterations in tocopherol cyclase activity in transgenic and mutant plants of Arabidopsis affect tocopherol content, tocopherol composition, and oxidative stress. *Plant Physiology* 137: 713–723.

Kessler F, Schnell D, Blobel G. 1999. Identification of proteins associated with plastoglobules isolated from pea (*Pisum sativum* L.) chloroplasts. *Planta* 208: 107–113.

Kim EH, Lee Y, Kim HU. 2015. Fibrillin 5 is essential for plastoquinone-9 biosynthesis by binding to solanesyl diphosphate synthases in Arabidopsis. *Plant Cell* 27: 2956–2971.

Koop HU, Steinmuller K, Wagner H, Rossler C, Eibl C, Sacher L. 1996. Integration of foreign sequences into the tobacco plastome via polyethylene glycol-mediated protoplast transformation. *Planta* 199: 193–201.

Kopriva S, Calderwood A, Weckopp SC, Koprivova A. 2015. Plant sulfur and big data. *Plant Science* 241: 1–10.

Koprivova A, Kopriva S. 2014. Molecular mechanisms of regulation of sulfate assimilation: first steps on a long road. *Frontiers in Plant Science* 5: e589.

Lichtenthaler HK. 1987. Chlorophylls and carotenoids – pigments of photosynthetic biomembranes. *Methods in Enzymology* 148: 350–382.

Lisec J, Schauer N, Kopka J, Willmitzer L, Fernie AR. 2006. Gas chromatography mass spectrometry-based metabolite profiling in plants. *Nature Protocols* 1: 387–396.

Liu X, Wu FH, Li JX, Chen J, Wang GH, Wang WH, Hu WJ, Gao LJ, Wang ZL, Chen JH *et al.* 2016. Glutathione homeostasis and Cd tolerance in the Arabidopsis *sultr1;1-sultr1;2* double mutant with limiting sulfate supply. *Plant Cell Reports* 35: 397–413.

Lloyd J, Meinke D. 2012. A comprehensive dataset of genes with a loss-of-function mutant phenotype in Arabidopsis. *Plant Physiology* 158: 1115–1129.

Luedemann A, Strassburg K, Erban A, Kopka J. 2008. TagFinder for the quantitative analysis of gas chromatography–mass spectrometry (GC–MS)-based metabolite profiling experiments. *Bioinformatics* 24: 732–737.

Lundquist PK, Poliakov A, Bhuiyan NH, Zybailov B, Sun Q, van Wijk KJ. 2012. The functional network of the Arabidopsis plastoglobule proteome based on quantitative proteomics and genome-wide coexpression analysis. *Plant Physiology* 158: 1172–1192.

Lundquist PK, Poliakov A, Giacomelli L, Friso G, Appel M, McQuinn RP, Krasnoff SB, Rowland E, Ponnala L, Sun Q *et al.* 2013. Loss of plastoglobule kinases ABC1K1 and ABC1K3 causes conditional degreening, modified prenyl-lipids, and recruitment of the jasmonic acid pathway. *Plant Cell* 25: 1818–1839.

Kauss D, Bischof S, Steiner S, Apel K, Meskauskiene R. 2012. FLU, a negative feedback regulator of tetrapyrrole biosynthesis, is physically linked to the final steps of the Mg^{++}-branch of this pathway. *FEBS Letters* 586: 211–216.

Monte E, Ludevid D, Prat S. 1999. Leaf C40.4: a carotenoid-associated protein involved in the modulation of photosynthetic efficiency? *The Plant Journal* 19: 399–410.

Nacir H, Brehelin C. 2013. When proteomics reveals unsuspected roles: the plastoglobule example. *Frontiers in Plant Science* 4: e114.

Neff MM, Chory J. 1998. Genetic interactions between phytochrome A, phytochrome B, and cryptochrome 1 during Arabidopsis development. *Plant Physiology* 118: 27–35.

Noctor G, Foyer CH. 1998. Ascorbate and glutathione: keeping active oxygen under control. *Annual Review of Plant Physiology and Plant Molecular Biology* 49: 249–279.

Noctor G, Mhamdi A, Chaouch S, Han Y, Neukermans J, Marquez-Garcia B, Queval G, Foyer CH. 2012. Glutathione in plants: an integrated overview. *Plant, Cell & Environment* 35: 454–484.

Noctor G, Reichheld JP, Foyer CH. 2018. ROS-related redox regulation and signaling in plants. *Seminars in Cell & Developmental Biology* 80: 3–12.

Otsubo M, Ikoma C, Ueda M, Ishii Y, Tamura N. 2018. Functional role of fibrillin5 in acclimation to photooxidative stress. *Plant and Cell Physiology* 59: 1670–1682.

Pnueli L, Liang H, Rozenberg M, Mittler R. 2003. Growth suppression, altered stomatal responses, and augmented induction of heat shock proteins in cytosolic ascorbate peroxidase (Apx1)-deficient Arabidopsis plants. *The Plant Journal* 34: 187–203.

Queval G, Noctor G. 2007. A plate reader method for the measurement of NAD, NADP, glutathione, and ascorbate in tissue extracts: application to redox profiling during Arabidopsis rosette development. *Analytical Biochemistry* 363: 58–69.

Rey P, Gillet B, Romer S, Eymery F, Massimino J, Peltier G, Kuntz M. 2000. Over-expression of a pepper plastid lipid-associated protein in tobacco leads to changes in plastid ultrastructure and plant development upon stress. *The Plant Journal* 21: 483–494.

Roessner U, Luedemann A, Brust D, Fiehn O, Linke T, Willmitzer L, Fernie A. 2001. Metabolic profiling allows comprehensive phenotyping of genetically or environmentally modified plant systems. *Plant Cell* 13: 11–29.

Romani I, Manavski N, Morosetti A, Tadini L, Maier S, Kuhn K, Ruwe H, Schmitz-Linneweber C, Wanner G, Leister D *et al.* 2015. A member of the Arabidopsis mitochondrial transcription termination factor family is required for maturation of chloroplast transfer RNA^{Ile}(GAU). *Plant Physiology* 169: 627–646.

Rosso MG, Li Y, Strizhov N, Reiss B, Dekker K, Weisshaar B. 2003. An *Arabidopsis thaliana* T-DNA mutagenized population (GABI-Kat) for flanking sequence tag-based reverse genetics. *Plant Molecular Biology* 53: 247–259.

Rottet S, Besagni C, Kessler F. 2015. The role of plastoglobules in thylakoid lipid remodeling during plant development. *Biochimica et Biophysica Acta (BBA) – Bioenergetics* 1847: 889–899.

Rung J, Brazma A. 2013. Reuse of public genome-wide gene expression data. *Nature Reviews Genetics* 14: 89–99.

Sattler SE, Gilliland LU, Magallanes-Lundback M, Pollard M, DellaPenna D. 2004. Vitamin E is essential for seed longevity and for preventing lipid peroxidation during germination. *Plant Cell* 16: 1419–1432.

Scharfenberg M, Mittermayr L, von Roepenack-Lahaye E, Schlicke H, Grimm B, Leister D, Kleine T. 2015. Functional characterization of the two ferrochelatases in *Arabidopsis thaliana*. *Plant, Cell & Environment* 38: 280–298.

Schwab R, Ossowski S, Riester M, Warthmann N, Weigel D. 2006. Highly specific gene silencing by artificial microRNAs in Arabidopsis. *Plant Cell* 18: 1121–1133.

Singh DK, Laremore TN, Smith PB, Maximova SN, McNellis TW. 2012. Knockdown of *FIBRILLIN4* gene expression in apple decreases plastoglobule plastoquinone content. *PLoS ONE* 7: e47547.

Singh DK, Maximova SN, Jensen PJ, Lehman BL, Ngugi HK, McNellis TW. 2010. *FIBRILLIN4* is required for plastoglobule development and stress resistance in apple and Arabidopsis. *Plant Physiology* 154: 1281–1293.

Singh DK, McNellis TW. 2011. Fibrillin protein function: the tip of the iceberg? *Trends in Plant Science* 16: 432–441.

Suzuki N, Miller G, Sejima H, Harper J, Mittler R. 2013. Enhanced seed production under prolonged heat stress conditions in *Arabidopsis thaliana* plants deficient in cytosolic ascorbate peroxidase 2. *Journal of Experimental Botany* 64: 253–263.

Szymanska R, Kruk J. 2010. Plastoquinol is the main prenyllipid synthesized during acclimation to high light conditions in Arabidopsis and is converted to plastochromanol by tocopherol cyclase. *Plant and Cell Physiology* 51: 537–545.

Takahashi H, Kopriva S, Giordano M, Saito K, Hell R. 2011. Sulfur assimilation in photosynthetic organisms: molecular functions and regulations of transporters and assimilatory enzymes. *Annual Review of Plant Biology* 62: 157–184.

Usadel B, Obayashi T, Mutwil M, Giorgi FM, Bassel GW, Tanimoto M, Chow A, Steinhauser D, Persson S, Provart NJ. 2009. Co-expression tools for plant biology: opportunities for hypothesis generation and caveats. *Plant, Cell & Environment* 32: 1633–1651.

van Wijk KJ, Kessler F. 2017. Plastoglobuli: plastid microcompartments with integrated functions in metabolism, plastid developmental transitions, and environmental adaptation. *Annual Review of Plant Biology* 68: 253–289.

Vidi PA, Kanwischer M, Baginsky S, Austin JR, Csucs G, Dörmann P, Kessler F, Brehelin C. 2006. Tocopherol cyclase (VTE1) localization and vitamin E accumulation in chloroplast plastoglobule lipoprotein particles. *Journal of Biological Chemistry* 281: 11225–11234.

Xu D, Leister D, Kleine T. 2017. *Arabidopsis thaliana* mTERF10 and mTERF11, but not mTERF12, are involved in the response to salt stress. *Frontiers in Plant Science* 8: e1213.

Xu D, Marino G, Klingl A, Enderle B, Monte E, Kurth J, Hiltbrunner A, Leister D, Kleine T. 2019. Extrachloroplastic PP7L functions in chloroplast development and abiotic stress tolerance. *Plant Physiology* 180: 323–341.

Yang Y, Sulpice R, Himmelbach A, Meinhard M, Christmann A, Grill E. 2006. Fibrillin expression is regulated by abscisic acid response regulators and is involved in abscisic acid-mediated photoprotection. *Proceedings of the National Academy of Sciences, USA* 103: 6061–6066.

Yonekura-Sakakibara K, Saito K. 2013. Transcriptome coexpression analysis using ATTED-II for integrated transcriptomic/metabolomic analysis. *Methods Molecular Biology* 1011: 317–326.

Youssef A, Laizet Y, Block MA, Marechal E, Alcaraz JP, Larson TR, Pontier D, Gaffe J, Kuntz M. 2010. Plant lipid-associated fibrillin proteins condition jasmonate production under photosynthetic stress. *The Plant Journal* 61: 436–445.

Ytterberg AJ, Peltier JB, van Wijk KJ. 2006. Protein profiling of plastoglobules in chloroplasts and chromoplasts. A surprising site for differential accumulation of metabolic enzymes. *Plant Physiology* 140: 984–997.

Zbierzak AM, Kanwischer M, Wille C, Vidi PA, Giavalisco P, Lohmann A, Briesen I, Porfirova S, Brehelin C, Kessler F *et al.* 2010. Intersection of the tocopherol and plastoquinol metabolic pathways at the plastoglobule. *Biochemical Journal* 425: 389–399.

Zhang R, Wise RR, Struck KR, Sharkey TD. 2010. Moderate heat stress of *Arabidopsis thaliana* leaves causes chloroplast swelling and plastoglobule formation. *Photosynthesis Research* 105: 123–134.

Supporting Information

Additional Supporting Information may be found online in the Supporting Information section at the end of the article.

Fig. S1 Supplemental phenotypic characterization of *Arabidopsis thaliana fbn6* T-DNA insertion mutants.

Fig. S2 Generation and phenotypic characterization of *Arabidopsis thaliana fbn6* amiRNA lines.

Fig. S3 Induction of non-photochemical quenching (NPQ) in *Arabidopsis thaliana* Col-0 and *fbn6-1* leaves.

Fig. S4 Transmission electron micrographs of ultrathin sections of *Arabidopsis thaliana* Col-0 and *fbn6-1* leaves of plants grown under 120 µmol photons $m^{-2} s^{-1}$.

Fig. S5 Behavior of *Arabidopsis thaliana* wild-type (Col-0) and plants lacking FBN6 under high light stress.

Fig. S6 Gene ontology (GO) analysis of genes whose expression is elevated or reduced in 3-wk-old *Arabidopsis thaliana* fbn6-1 plants compared to Col-0.

Table S1 Primers used in this study.

Table S2 Expression correlation analysis with the Arabidopsis Co-expression Tool in ATTED-II to determine the level of co-expression between *FBN6* and all other genes represented on the ATH1 microarray (22K) chip.

Table S3 Segregation analysis of the F2 offspring of *Arabidopsis thaliana fbn6-1* back-crossed to Col-0.

Table S4 Identification of *Arabidopsis thaliana* mutants with an *fbn6-1*-like phenotype by filtering a dataset published by Lloyd & Meinke (2012).

Table S5 Genes whose transcript levels were significantly regulated in 3-wk-old *Arabidopsis thaliana fbn6-1* seedlings compared to Col-0.

Table S6 GC-MS analysis of 3-wk-old *Arabidopsis thaliana* wild-type (Col-0) and *fbn6-1* mutant plants grown under 120 µmol photons $m^{-2} s^{-1}$.